



1 **Current and Future Rainfall-Driven Flood Risk From**
2 **Hurricanes in Puerto Rico Under 1.5°C and 2°C Climate**
3 **Change**

4 Leanne Archer¹, Jeffrey Neal¹, Paul Bates¹, Emily Vosper¹, Dereka Carroll², Jeison Sosa³,
5 Daniel Mitchell¹

6 ¹School of Geographical Sciences, University of Bristol, Bristol, UK

7 ²Department of Chemistry, Physics, and Atmospheric Sciences, Jackson State University, Jackson MS, United
8 States

9 ³Fathom, Bristol, UK

10 *Correspondence to:* Leanne Archer (leanne.archer@bristol.ac.uk)

11
12 **Abstract**

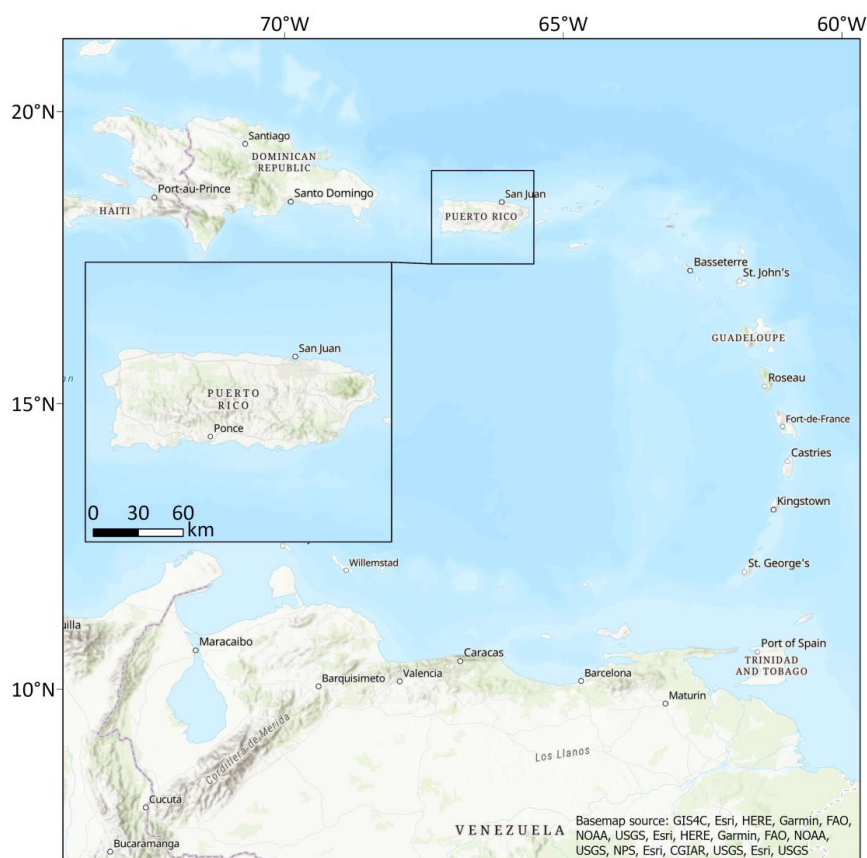
13 Flooding associated with Hurricane Maria in 2017 had devastating consequences for lives and livelihoods in
14 Puerto Rico. Yet, an understanding of current and future flood risk in small islands like Puerto Rico is limited.
15 Thus, efforts to build resilience to flooding associated with hurricanes remain constrained. Here, we take an
16 event set of hurricane rainfall estimates from a synthetic hurricane rainfall simulator as the input to an event-
17 based rainfall-driven flood inundation model using hydrodynamic code LISFLOOD-FP. Validation of our
18 model against High Water Mark data for Hurricane Maria demonstrates the suitability of this model for
19 estimating flood hazard in Puerto Rico. We produce event-based flood hazard and population exposure
20 estimates for the present day, and the future under the 1.5°C and 2°C Paris Agreement goals. Population
21 exposure to flooding from hurricane rainfall in Puerto Rico for the present day climate is approximately 8-10%
22 of the current population for 5-year return period, with an increase in population exposure to flooding by 2-15%
23 and 1-20% under 1.5°C and 2°C futures (5-year return period). This research demonstrates the significance of
24 the 1.5°C Paris Agreement goal for Small Island Developing States, providing the first event-based estimates of
25 flooding from hurricane rainfall under climate change in a small island.

26 **1 Introduction**

27 Climate change is amplifying the probability of high intensity tropical cyclone events globally (Patricola and
28 Wehner, 2018; Kossin et al., 2020; Mei and Xie, 2016; Knutson et al., 2020), compounding the rising social and
29 economic costs associated with disasters due to increasing population and asset exposure (Jiménez Cisneros et
30 al., 2014). The adoption of the Paris Agreement in 2015 aimed to limit global warming to well below 2°C above
31 pre-industrial levels, and if possible to 1.5°C (United Nations Framework Convention on Climate Change,
32 2015). Following this, numerous studies have investigated how these global temperature changes could impact
33 societies, ecosystems, and places (IPCC, 2018; Mitchell et al., 2016). Under the upper Paris Agreement goal of
34 2°C, there will likely be a higher proportion of tropical cyclones that become the most intense storms (i.e.
35 Category 4 and 5 hurricanes), with an increase in precipitation intensity (Knutson et al., 2020). Whilst flooding
36 accounts for the largest proportion of loss of life and economic damages from tropical cyclones (Rappaport,
37 2014; Czajkowski et al., 2017), there is a lack of literature exploring how flooding might be affected by changes
38 in tropical cyclone characteristics under climate change. This is particularly pertinent for Small Island



39 Developing States where the difference between the 1.5°C and 2°C temperature goals may be critically
40 important (Hoegh-Guldberg et al., 2018).
41
42 Small Island Developing States (SIDS) are a group of small island nations and territories with an acute risk of
43 disasters and the impacts of climate change, who were an instrumental force in the implementation of the 1.5°C
44 goal in the Paris Agreement (Ourbak and Magnan, 2018). Considering risk as a function of hazard, exposure and
45 vulnerability (Terminology, 2019), high hazard frequency, high exposure in relation to size and underlying
46 vulnerabilities drive the risk of hydrometeorological disasters and climate change in SIDS (Nurse et al., 2014;
47 Mycoo et al., 2022). Climate change is likely to exacerbate current flood risk in SIDS (Joyette et al., 2014;
48 Thomas et al., 2017) based on projected changes in tropical cyclone precipitation (Vosper et al., 2020),
49 increased coastal storm surge heights (Knutson et al., 2020; Monioudi et al., 2018) and sea level rise (Storlazzi
50 et al., 2018; Nicholls et al., 2018; Rasmussen et al., 2018). Yet, very little island-scale quantitative assessment of
51 flood risk has been conducted in SIDS. This is largely due to the inadequacy of existing methods as well as
52 insufficient data resolution and quality suitable for the scale of small island modelling (typically <10,000km²)
53 (Thomas et al., 2019).
54
55 Recent work by Vosper et al., (2020) demonstrates that total rainfall associated with tropical cyclones (also
56 known as hurricanes) in the Caribbean will increase under both the 1.5°C and 2°C Paris Agreement goals in
57 comparison to the present day climate. They also estimate that a 100-year return period event similar to
58 Hurricane Maria in Puerto Rico would be twice as likely to occur under the 2°C scenario than the 1.5°C scenario
59 (Vosper et al., 2020). Puerto Rico is an unincorporated territory of the United States located in the Greater
60 Antilles islands of the Caribbean (see Figure 1). The urgent need to understand both current and future flood risk
61 was recently reinforced following Hurricane Maria in 2017, which made landfall as a high-end Category 4
62 hurricane, causing catastrophic wind and flood damage (Pasch et al., 2018). Hurricane Maria was the strongest
63 hurricane to hit Puerto Rico since Hurricane San Felipe II in 1928, resulting in at least 2975 deaths (Audi et al.,
64 2018). The estimated economic loss of US\$90 billion made it the third costliest disaster in US history (Pasch et
65 al., 2018). Despite the underlying structural failures and inadequate emergency response that also contributed to
66 the scale of the disaster in Puerto Rico (Towe et al., 2020; Rivera, 2020; Caban, 2019; Willison et al., 2019), the
67 volume and intensity of the rainfall associated with Hurricane Maria was unprecedented and exacerbated the
68 scale of the impact on communities on the island (Keellings and Hernández Ayala, 2019; Ramos-Scharrón and
69 Arima, 2019). Historically, hurricane rainfall has been the key cause of flooding in Puerto Rico (Hernández
70 Ayala et al., 2017; Smith et al., 2005). Consequently, it is pertinent that estimates of current and future rainfall-
71 driven flood risk associated with these hurricane rainfall events are developed to assist disaster risk management
72 in Puerto Rico. Yet, there are currently no complete estimates of flooding associated with Hurricane Maria, or
73 indeed for any other events in Puerto Rico. Dated FEMA flood zone maps do exist for larger river systems in
74 Puerto Rico, but these do not include pluvial flooding which is a key focus of this paper. They are therefore
75 likely to provide a considerable underestimate of risk (Wing et al., 2017).



76

77 **Figure 1 - Map showing the island of Puerto Rico within the Caribbean region.**

78

79 Tropical cyclones can generate pluvial, fluvial and coastal floods, all of which interact. Of these pluvial flooding
80 is a comparatively lesser modelled phenomenon (Blanc et al., 2012; Rözer et al., 2019; Tanaka et al., 2020).

81 Pluvial flooding is defined here as ‘flooding resulting from rainfall-generated overland flow and ponding before
82 the runoff enters any watercourse or drainage system, or cannot enter it because the network is full to capacity’
83 (Falconer et al., 2009, p.199). There has been a historical split between the modelling and assessment of pluvial
84 and fluvial – or river - flooding. However, in reality both of these inland flood types are in a continuum, and
85 both driven by rainfall. Thus, the distinction between the two is unhelpful in many cases. This is particularly
86 true in small islands where much of the inland flooding is primarily driven by heavy rainfall (Jetten, 2016;
87 Burgess et al., 2015). Pluvial flooding is also a contested term, with some defining it as including small river
88 channels (Wing et al., 2018), and other defining it as completely independent of rivers (Rosenzweig et al., 2018;
89 Hankin et al., 2008). The rain on grid approach documented here therefore overcomes this pluvial/fluvial
90 distinction by explicitly modelling both flood types and their interactions. Here we define the flooding modelled
91 in this approach as ‘rainfall-driven flooding’.

92



93 Rainfall-driven flood events can often occur with a high frequency but low magnitude. This can lead to a
94 significant cumulative impact on a community's resilience over time which can undermine efforts to reach the
95 UN's Sustainable Development Goals (Moftakhari et al., 2017; Hamdan, 2015; United Nations Office for
96 Disaster Risk Reduction, 2019). However, most studies investigating flooding under climate change focus on
97 changes in the 100-year flood extent because this is often used as a design standard (Hirabayashi et al., 2013;
98 Arnell and Gosling, 2016; Lehner et al., 2006). This means the critical understanding of how smaller, more
99 frequent events might vary under climate change remains, which have a crucial importance for improving the
100 resilience-building and climate change adaptation needed in local communities (Moftakhari et al., 2017). This
101 paper aims to address this gap by investigating how changing hurricane rainfall characteristics influence
102 rainfall-driven flood risk estimates in Small Island Developing State Puerto Rico, with an emphasis on
103 understanding changes in lower magnitude, higher frequency events (<30-year return period).

104

105 Currently, the predominant method for understanding changes in flooding under climate change in small islands
106 uses changes in precipitation as a proxy for changes in flood hazard, leading to uncertainty in flood hazard
107 changes under climate change (Seneviratne et al., 2021; Ranasinghe et al., 2021). Examples of pluvial hydraulic
108 flood modelling in small islands have previously relied on spatially uniform rainfall estimates derived from
109 historical data for a set of design return period events (World Bank, 2015; Pratomo et al., 2016; Lumbroso et al.,
110 2011). This approach takes a set of rainfall intensity estimates for a given duration and return period, often
111 derived from an Intensity-Duration-Frequency (IDF) curve using historical rainfall data. Rainfall is typically
112 applied uniformly across a model domain to produce design event flood extents (World Bank, 2015). Yet, this
113 approach does not necessarily represent flooding at a particular return period, as a flood is a signature of the
114 rainfall, the topography and the topology of a catchment (Guerreiro et al., 2017; Skougaard Kaspersen et al.,
115 2017). More recently, studies have highlighted the importance of representing rainfall spatially and temporally
116 for a more realistic representation of flooding (Aldridge et al., 2020; Bernet et al., 2019; Guerreiro et al., 2017;
117 Schaller et al., 2020). One way of incorporating these features is through an 'event set approach', which
118 involves utilizing an event set of synthetic rainfall events (Nuswantoro et al., 2016; Tanaka et al., 2020).
119 Nonetheless, data such as this are still limited or non-existent – particularly in small islands – and thus the
120 aforementioned traditional approach has until now the only way to represent flood hazards for small islands.
121 Climate change is often assessed by applying an uplift factor to account for changes in rainfall associated with
122 climate change projections (Sayers et al., 2020). However, this approach also fails to account for non-stationary
123 effects of climate change on flooding, including changes to the different spatial and temporal characteristics of
124 rainfall that are important for flood generation (Rosenzweig et al., 2018).

125

126 This paper details the first example of an event-based assessment of flood hazard in a small island under current
127 and future climate change. We utilise a synthetic hurricane rainfall data set (Vosper et al., 2020) as the input to
128 an event-based rainfall-driven hydrodynamic flood model of Puerto Rico. We model rainfall-driven flood
129 hazard and population exposure at the island scale in Puerto Rico (9100km²), at 20m resolution under present
130 day, 1.5°C and 2°C climate change. As part of this work, we also include novel methodological developments,
131 including the representation of rainfall and river channels in the model. The model is validated against flood
132 hazard simulations using two estimates of Hurricane Maria observed rainfall (IMERG and NCEP Stage IV) and



133 High Water Mark data collected from the event. To our knowledge, these are the first published estimates of
134 rainfall-driven flooding from Hurricane Maria. This work thus demonstrates a step-change in the capacity to
135 estimate flood hazard in a small island, superseding the information available using the traditional approaches.

136 Within this, two key questions will be investigated:

- 137 1) What is the current rainfall-driven flood hazard and population exposure associated with hurricanes in
138 Puerto Rico?
- 139 2) How does population exposure to flooding change from present day under 1.5°C and 2°C climate
140 change scenarios?

141 **2 Methods**

142 To address these questions, we first describe the application of the hurricane rainfall event set in Section 2.1. We
143 explain how the event-based model was set up (Section 2.2), including the novel methodological applications of
144 spatially-varying rainfall in the hydrodynamic model (Section 2.2.1), and the parameterization of river channel
145 bathymetry using the input rainfall event set climatology (Section 2.2.2). In Section 2.3, we describe the
146 combination of population estimates with the flood hazard data to derive population exposure estimates under
147 present day, 1.5°C and 2°C climate change scenarios. The method for validating the model is described in
148 Section 2.4.

149

150 **2.1 Hurricane Rainfall Data**

151 The synthetic hurricane rainfall event set was developed to estimate hurricane rainfall in the Caribbean under
152 present day (2005-2016), 1.5°C and 2°C equilibrated climate change, using a physics-based tropical cyclone
153 rainfall model (Vosper et al., 2020). The model produces spatial (10km resolution) and temporal (2-hourly)
154 rainfall estimates along a synthetic hurricane track, considering four key rainfall-generating mechanisms: wind
155 shear, topography, vortex stretching and surface frictional convergence. Inputs to the tropical cyclone rainfall
156 model were atmospheric temperature, specific humidity, sea surface temperature and wind vectors, which are
157 typically taken from global climate models or reanalysis products. This model has been validated against gauge-
158 based and radar observations in several studies in the US - including in Puerto Rico - showing good agreement
159 (Feldmann et al., 2019; Lu et al., 2018; Zhu et al., 2013).

160

161 To provide driving climate model data to the synthetic hurricane rainfall events under current, 1.5°C and 2°C
162 climate change, four climate models from the Half A degree additional warming, Prognosis and Projected
163 Impacts (HAPPI) ensemble were utilised (CanAM4, CAM5-1-2-025degree, NorESM1-HAPPI, ECHAM6-3-
164 LR: (Mitchell et al., 2017)). These were selected based on the availability of variables at the required
165 atmospheric levels with at least daily temporal resolution for input into the hurricane rainfall model. HAPPI was
166 developed to document climate change impacts under 1.5°C and 2°C climate change above pre-industrial levels,
167 and has been a key source of climate data for such studies, including the IPCC Special Report on 1.5°C (IPCC,
168 2018). The hurricane rainfall event set consists of 59,000 events, with each climate model scenario equivalent to
169 between 332-427 simulated years of data depending on the climate model (Vosper et al., 2020). 59,000 events
170 were generated corresponding to approximately 5000 events per climate model and climate scenario. For each
171 climate model, the number of simulated years was calculated as the sum of the number of simulated events per
172 year divided by the simulated annual frequency of events in the climate model data. The simulated time period



173 for the present day is 2005-2016, representing a global average temperature of around 0.9°C higher than a pre-
174 industrial climate. The 1.5°C and 2°C time periods are for 2106-2115. Each synthetic hurricane rainfall event
175 was simulated at a 2-hour time step and 10km spatial resolution before being employed as the input to the event-
176 based rainfall-driven flood model.

177 **2.2 Event-Based Rainfall-Driven Flood Model**

178 LISFLOOD-FP is the hydraulic engine used to simulate channel and floodplain flow in two dimensions in our
179 rainfall-driven hydrodynamic model (Bates et al., 2010; LISFLOOD-FP Developers, 2020). Rainfall is the key
180 input to the model, and water flow is routed in one of two ways. Firstly, very shallow (<1cm) overland flows are
181 routed using a constant-velocity 'rain on grid' routing scheme (Sampson et al., 2013). Rain falls directly onto
182 the cells and is routed through the model using a slope-dependent fixed velocity algorithm. Secondly, flow
183 above 1cm deep (i.e. the majority) is routed hydraulically using the inertial form of the shallow water equations
184 (Bates et al., 2010), with river and drainage channels represented using a subgrid approach (Neal et al., 2012).
185 Typical channel (0.035) and floodplain (0.040) manning's coefficient friction values were applied. As Puerto
186 Rico is an island, all downstream boundaries are the ocean. The downstream boundary conditions in the model
187 are set to sea level, and this could be used in future work to simulate sea level rise and storm surge.

188

189 As Digital Elevation Data is the most important input to a hydrodynamic model (Hawker et al., 2018), LiDAR
190 data was used as the Digital Elevation Model (DEM). LiDAR coverage for Puerto Rico is almost complete
191 (>99%) (United States Geological Survey, 2017) and was resampled from its native 1m resolution to 20m,
192 reprojected to WGS84 and hydrologically conditioned using the Priority-flood method (Zhou et al., 2016). The
193 ~55km² of Puerto Rico not covered by LiDAR was patched with the globally-available MERIT DEM
194 (Yamazaki et al., 2017). This area is mountainous and sparsely populated, meaning the use of MERIT here does
195 not affect the exposure results.

196

197 Whilst high resolution DEMs are important for simulating floods, halving the model grid resolution leads to an
198 increase in simulation time by an order of magnitude (Savage et al., 2016). For example, run on a 2 x 2.6GHz 8-
199 core Intel E5-2670 one example model in this event set for the 9100km² domain covering the entire island of
200 Puerto Rico takes 3 minutes to run at 90m, 77 minutes at 20m, approximately 770 minutes (12.8 hours) at 10m
201 and 7700 minutes (5.3 days) at 1m resolution. As a result, and given we have thousands of events to simulate,
202 the event set was run at 20m. This resolution balances the need for high resolution flood hazard outputs with the
203 computational costs associated with employing a high-resolution event-based model at the island scale, and also
204 reflects state-of-the-art model resolutions used in other locations, such as the UK (Bates et al., 2023). Our study
205 is the first known study to employ an event set approach at such a high hydrodynamic model resolution over
206 such a large domain.

207

208 Infiltration was not included in this model approach for several reasons. As hurricanes take place during the
209 hurricane season (North Atlantic: June – November), soils in Puerto Rico are often saturated meaning
210 infiltration is low (Smith et al., 2005). Many pluvial modelling studies do not include infiltration as the
211 appropriate parameter values are highly uncertain and vary widely across space and time (Bernet et al., 2018;
212 Guerreiro et al., 2017; Hall, 2015). Although antecedent conditions are expected to vary, the infiltration is likely



213 to be of lower importance relative to other factors since infiltration will be minimal under extreme rainfall
214 events - such as those associated with hurricanes (Wehner and Sampson, 2021).

215

216 To improve the representation of islands and hurricane rainfall in the model, two novel model developments
217 were incorporated into the model set up.

218 **2.2.1 Spatially-varying Rainfall**

219 Spatiotemporal representation of rainfall is important for accurate simulation of pluvial flood events (Blanc et
220 al., 2012). Previous pluvial models using LISFLOOD-FP covered only small domains and relied on time-
221 varying but spatially constant rainfall input (Sampson et al., 2013, 2015; Wing et al., 2019). This study
222 demonstrates the first use of spatially and time-varying rainfall in a LISFLOOD-FP rainfall-driven
223 hydrodynamic model, using a new routine to read spatiotemporal rainfall in NetCDF format. For each hurricane,
224 a grid of rainfall at ~10km resolution across the island was input to the model domain at each timestep (2-
225 hourly), although the hydrodynamic model calculations are simulated with much shorter timesteps (order of
226 seconds). To model all 59,000 hurricane rainfall events would be computationally intractable, and was not
227 necessary considering many of the hurricane rainfall events produced no or very little rainfall. Thus, to select
228 events to simulate in the model, all hurricane rainfall events above a threshold of 3.75mmhr^{-1} peak rainfall
229 intensity were simulated - a total of 4909 events (8.3% of total). Within this, 1464 events were present day, 1801
230 events were at 1.5°C and 1644 events were at 2°C . This threshold was selected as the minimum number of
231 events necessary to calculate a robust estimate of the two-year return period flood hazard which is used as the
232 lowest modelled return period event in the event set. Events below this threshold were not considered significant
233 enough in terms of rainfall to run. An additional 8 hours of simulation time was added to the end of each
234 simulation based on our inspection of the time it took for the rainfall to move through the model and reach either
235 the ocean or the lowest points of the DEM. These decisions were based on trial and error and inspection of the
236 rainfall and resulting flood hazard events.

237 **2.2.2 River Channels**

238 Including river channels in flood models is necessary to produce accurate estimates of flood hazard (Hall, 2015;
239 Neal et al., 2021), but most pluvial flood models do not explicitly include river channels or drainage networks
240 (Blanc et al., 2012). Here, a subgrid approach was used to represent river channels and drainage networks in the
241 rainfall-driven modelling framework (Neal et al., 2012). Rivers and drainage channels were represented using
242 the US National Hydrography Dataset v2.1 (Simley and Carswell Jr, 2010). River widths in Puerto Rico are
243 inadequately represented in global hydrographic datasets such as MERIT Hydro (Yamazaki et al., 2019) as most
244 channels are smaller than the resolution of the DEM data used to create such products (e.g. MERIT at 90m in
245 the case of MERIT-Hydro). As a result, width was estimated using a power law regression with upstream
246 accumulated area (Leopold and Maddock, 1953). Widths used here were sampled using satellite imagery along
247 the 13 main rivers across the island. Upstream accumulated area was calculated using the LiDAR DEM at 20m
248 resolution by first generating a flow direction map, and then using the RichDEM algorithm outlined in (Barnes,
249 2017).

250



251 River depth estimates are also unavailable for Puerto Rico, as is typical in most locations globally (Sampson et
252 al., 2015). To parameterise the river channel depths, the present day synthetic hurricane rainfall events for each
253 climate model (total: 1464) were first simulated through a model with arbitrarily deep river channels (-10m) to
254 get estimates of channel water depth for each event. Using these, the water depth at a given return period was
255 calculated empirically. Information on flood defences was also not available, so in this study we parametrize
256 bankfull river depth by calculating the bed elevation to ensure that each channel conveyed the present day one-
257 in-two-year discharge (Pickup and Warner, 1976; Williams, 1978; Wolman and Miller, 1960) generated by the
258 present day hurricane ensemble and subtracted from the bank height derived from the DEM to get a calibrated
259 estimate of the channel depth value. Inevitably this means that in locations where rivers do have defences, the
260 model is likely to overpredict flood hazard. If defence standard information were to become available, it would
261 be a simple matter to retrospectively apply these to the output flood hazard layers.
262

263 **2.3 Population Exposure Estimates**

264 Population exposure was calculated for each flood event as the total number of people exposed to flood depths
265 above 10cm. The WorldPop 90m top-down constrained population dataset (2020) was used to estimate the
266 number of people per 90m grid cell (Tatem, 2017; Bondarenko et al., 2020). WorldPop was chosen because total
267 population estimates are adjusted to 2020 UN population estimates, meaning out-migration trends following
268 Hurricane Maria in 2017 are accounted for. The WorldPop data was downscaled from 90m to 20m to match the
269 flood hazard data, using nearest neighbour resampling and assignment to 20m cells based on a proportional cell
270 method, following (Lloyd et al., 2017). WorldPop has been validated and compared to other datasets extensively
271 (Reed et al., 2018; Leyk et al., 2019; Tuholske et al., 2021), including for flood exposure applications
272 (Mazzoleni et al., 2020; Smith et al., 2019). Smith et al., (2019) found that WorldPop produces larger exposure
273 estimates in comparison to the High Resolution Settlement Layer (HRSL) (Tiecke et al., 2017), likely due to a
274 combination of coarser resolution and assignment of population to buildings. Recently, Tuholske et al., (2021)
275 identified the importance of conducting a sensitivity assessment of gridded population products to capture the
276 inherent uncertainties in the use of gridded population estimates. However, HRSL, High Resolution Population
277 Density Map (HRPDM) (Mapping the world to help aid workers, with weakly, semi-supervised learning, 2020)
278 and WorldPop are likely to give different estimates in our case, not least due to the different dates of the datasets
279 before and after Hurricane Maria, where approximately 8% (230,000) of the population is estimated to have
280 emigrated following the event (Audi et al., 2018). Total population estimates for the main island using HRPDM
281 and HRSL population are 4.87million and 3.66million, which is considerably higher than the UN-adjusted
282 WorldPop estimate of 2.70million, resulting in higher population exposure values. Future population was not
283 considered due to a lack of available high-resolution datasets (<100m grid size) estimating changes in future
284 population. For consistency, population exposure exceedance was calculated for each event using the same
285 method as the hurricane rainfall as 1/Annual Exceedance Probability (Emanuel and Jagger, 2010; Feldmann et
286 al., 2019; Vosper et al., 2020).
287



288 **2.4 Model Validation**

289 To determine the skill of our flood hazard estimation, we assessed model performance using high water mark
290 (HWM) data collected by USGS following Hurricane Maria (available here:
291 <https://stn.wim.usgs.gov/FEV/#MariaSeptember2017>). For more information about the suitability assessment of
292 the HWM data for validation, see Text S1 and Table S2. See Figure S1 for the HWM locations used in this
293 study. Ideally it would be better to validate the event set with a lower magnitude flood considering the focus of
294 this work is primarily on low-magnitude, high-frequency events. However, there is no known validation data
295 for small hurricane rainfall-driven flood events in Puerto Rico. As a result, Hurricane Maria was chosen as the
296 event to validate against despite its high magnitude.

297

298 Firstly, to produce flood hazard estimates of Hurricane Maria for validating the model and event set, we ran the
299 hydrodynamic model using two observational rainfall products (IMERG and NCEP Stage IV) that provide
300 space-time varying estimates of Hurricane Maria rainfall through the flood inundation model. We use an
301 identical hydrodynamic model set-up to the event set, only changing the input rainfall data. IMERG (IMERG:
302 Integrated Multi-satellitE Retrievals for GPM | NASA Global Precipitation Measurement Mission, 2023) was
303 run at ~10km spatial resolution, and at 30-min intervals, whilst NCEP Stage IV (NCEP/EMC 4KM Gridded
304 Data (GRIB) Stage IV Data, 2023) was run at ~4km spatial resolution, with an hourly temporal resolution. We
305 compare the flood hazard produced using IMERG and NCEP Stage IV to understand the uncertainty in flood
306 hazard estimates using the different observation inputs.

307

308 Next, we compared the performance of the event set against the HWM data and the estimates from the observed
309 rainfall products to sense check the model. Hurricane Maria-like events were identified across all model
310 scenarios first by maximum total rainfall, and then by spatial characteristics of the hurricane track. Maximum
311 total rainfall is defined as the highest total rainfall accumulation at a point on the island. This metric was used as
312 opposed to mean total rainfall, as studies that have investigated Hurricane Maria rainfall describe the maximum
313 total rainfall as the most significant anomaly in the historical record associated with the event (Ramos-Scharrón
314 and Arima, 2019; Keellings and Hernández Ayala, 2019; Pokhrel et al., 2021). Maximum total rainfall is also
315 the metric used to estimate the return period of Hurricane Maria rainfall; at least a 1-in-15-year rainfall event
316 (Keellings and Hernández Ayala, 2019). Studies use different metrics to derive maximum total rainfall,
317 including interpolation of rain gauge data and observation products such as NCEP Stage IV. This means that the
318 maximum total rainfall for Hurricane Maria varies between studies, ranging between 733-1029mm (Pasch et al.,
319 2018; Keellings and Hernández Ayala, 2019; Ramos-Scharrón and Arima, 2019; Pokhrel et al., 2021). There are
320 a limited number of events in our event set with a >100-year return period magnitude maximum total rainfall
321 (mean: 3.46 samples per climate model scenario) due to the comparatively short simulated time record of our
322 event set (range: 332-427 years). However, Puerto Rico experiences on average one hurricane each year, and
323 has a mean annual rainfall of over 4000mm in some locations (Hernández Ayala and Matyas, 2016). There are
324 therefore many events in the event set with total mean rainfall (total accumulated rainfall averaged across the
325 island) in the range of Hurricane Maria (range: 375-380mm (Pokhrel et al., 2021; Keellings and Hernández
326 Ayala, 2019; Ramos-Scharrón and Arima, 2019)). However, these events have widely varying spatial
327 characteristics and associated flood hazard and are therefore not all are Maria-like. Thus, it is also important to



328 consider the spatial characteristics of the hurricane rainfall events so that events with similar rainfall and spatial
329 characteristics to Hurricane Maria can be identified. Similarity to Hurricane Maria based on track location was
330 assessed based on four criteria: i) direct landfall on the main island; ii) south-western trajectory; iii) makes
331 landfall on the eastern portion of the main island; and iv) similar track trajectory across the island, whereby the
332 event track and Hurricane Maria track intersect at at least one point on the island.

333 3 Results

334 3.1 Hurricane Maria Model Validation

335 Figure 2 shows the flood hazard estimates produced by simulating the IMERG and NCEP Stage IV rainfall
336 products spatiotemporally through the flood inundation model from the island to local scale. The RMSE
337 between the modelled flood hazard and the HWM is 1.18m for IMERG and 1.22m for NCEP Stage IV (see
338 Figure 3). This is comparable to post-event HWM validation done in other locations (Wing et al., 2021) (see
339 Section 4.1 for discussion of this). There is a significant difference in the flood extents produced using IMERG
340 and NCEP Stage IV, with larger areas flooded using NCEP Stage IV than IMERG. This highlights the
341 uncertainty in so-called ‘observed’ flooding from Hurricane Maria.

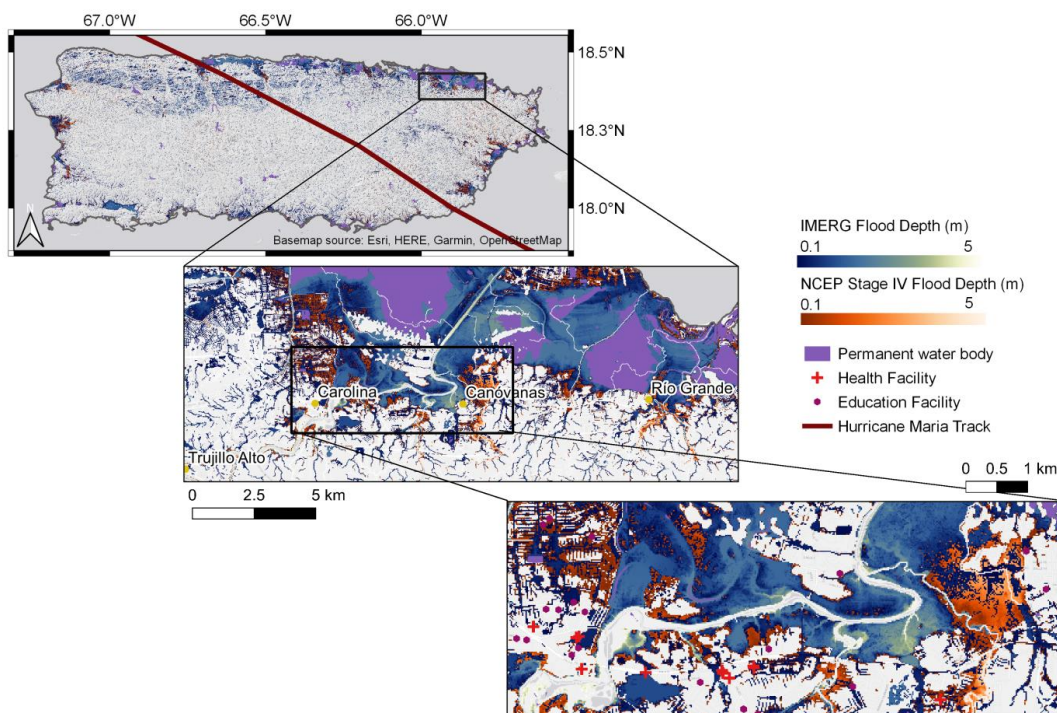


Figure 2 - Map showing the differences between flood hazard estimates of Hurricane Maria produced using IMERG and NCEP Stage IV precipitation data from the island to local scale.

342



343 In the event set, when the spatial characteristics of the hurricane rainfall events are considered in addition to the
344 maximum total rainfall, events we select as Hurricane Maria-like events have some of the lowest RMSEs
345 between the observed and modelled water surface elevations (range: 1.13-1.33m) as demonstrated in Figure 3.
346 The track locations of these events are shown in Figure S2. The relationship between maximum total rainfall
347 and RMSE for all events is expected, whereby as the intensity of the event increases, the sensitivity to the flood
348 depths decreases as the floodplain fills and thus becomes less responsive to additional increases in rainfall
349 (Wing et al., 2021). However, there are events in the event set with both much higher and lower rainfalls than
350 Hurricane Maria that have both similar and very different RMSEs to the Maria-like events. This demonstrates
351 the importance of the spatial characteristics of the events beyond just the rainfall.

352

353 When comparing the flood estimates using IMERG and NCEP Stage IV against the High Water Mark data, the
354 event set Maria-like events have similar RMSE scores (Figure 3). However, both observational rainfall products
355 have different maximum total rainfalls than those found in the literature. In particular, the IMERG maximum
356 total rainfall is considerably lower. This is likely because satellite products such as IMERG often underestimate
357 orographic rainfall such as that exhibited over Puerto Rico (Dinku et al., 2008).

358

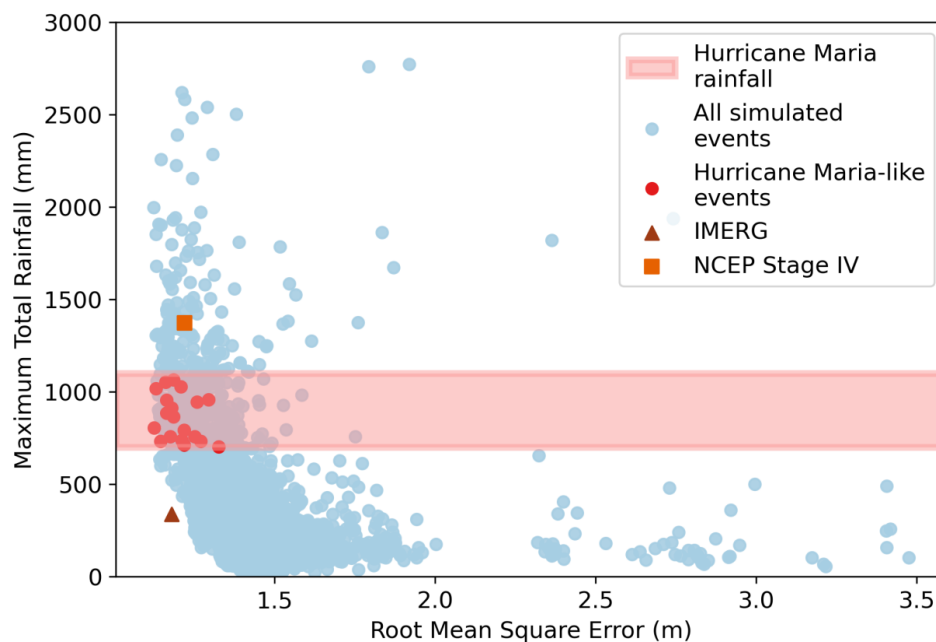


Figure 3 - Graph showing the relationship between Root Mean Square Error (RMSE) and maximum total rainfall for all simulated events under all climate scenarios (4909 events total). Blue = all simulated events. Red = events identified with Hurricane Maria maximum rainfall totals and spatial characteristics (20 events). Red band = range of reported Hurricane Maria rainfall. Orange square = NCEP Stage IV model. Brown triangle = IMERG model.



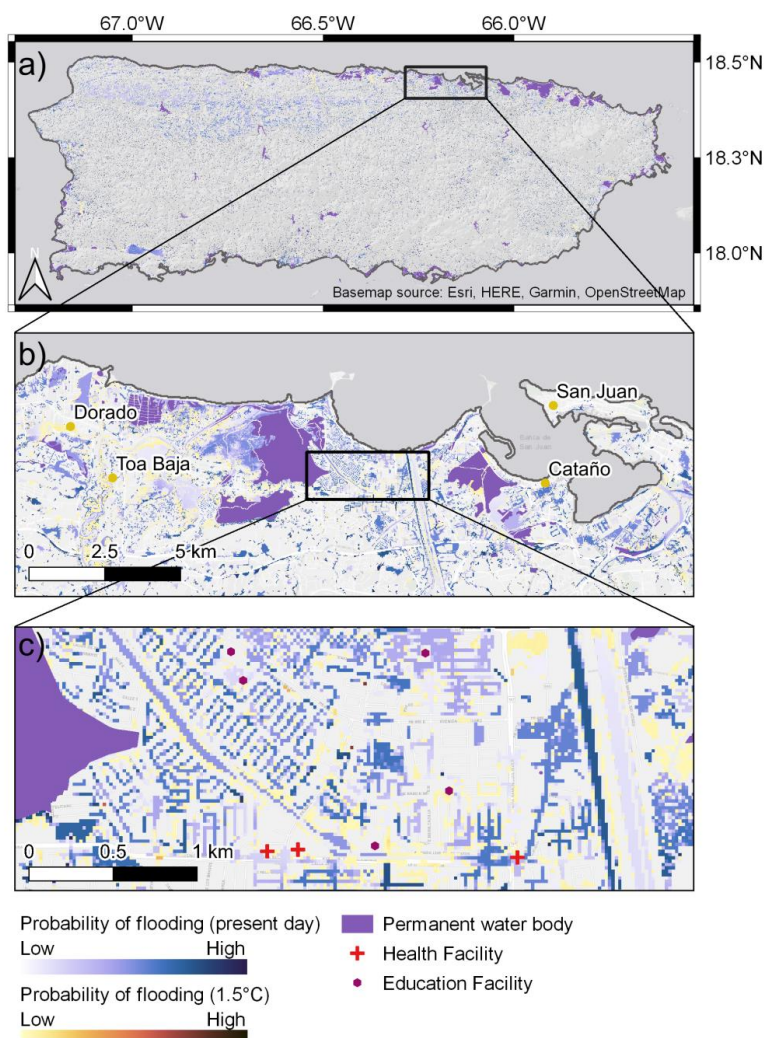
359 **3.2 Design Return Period Flood Hazard Maps**

360 The probability of inundation was calculated for each pixel in the model domain, calculating how many times
361 each pixel would be inundated above a 10cm depth in each climate model temperature scenario. The return
362 period of inundation in each pixel was then determined, by calculating how many times we expect a pixel to
363 flood based on the number of years of data simulated (range: 332-427 years depending on the climate model).
364 Using this, we derived a set of return period flood hazard maps, which provide a spatially explicit representation
365 of a given return period flood event under present day, 1.5°C and 2°C warming. This supersedes any currently
366 available hurricane rainfall-driven flood risk information in Puerto Rico, both under current and future climate
367 change. This approach also moves beyond the traditional uplift approach often used in flood risk assessment
368 under climate change, as it provides spatially explicit flood hazard information for a given return period at the
369 island scale and at high resolution.

370

371 Figure 4 highlights the scale and detail of flood hazard information using this approach, from the island scale
372 (Figure 4a) to the local scale (Figure 4c). For example, Figure 4c shows flooding at the street level in Levittown,
373 Toa Baja – a town significantly impacted by flooding from Hurricane Maria in 2017 (Major Hurricane Maria -
374 September 20, 2017).

375



376

377 **Figure 4 - Map showing the 20-year return period flood based on probability of inundation under present day and**

378 **1.5°C climate change for the ECHAM6-3-LR climate model. a) Flooding at the island scale. b) Flooding in the Toa**

379 **Baja and Cataño districts. c) Flooding in Levittown, Toa Baja. For presentation purposes, only inundation**

380 **probabilities at present day and 1.5°C are shown here.**

381 Based on this example for a 20-year return period flood hazard event using the ECHAM6-3-LR climate model,

382 several schools and hospitals would likely be impacted under present day and 1.5°C climate change. The

383 estimated flooded area of the 20-year return period flood increases under 1.5°C climate change in comparison to

384 present day (2006-2015) (Figure 4c), meaning areas currently not at risk are affected at 1.5°C climate change.

385 Changes at 2°C are similar to 1.5°C, but are not shown in Figure 4 for presentation purposes.

386

387 Flooding in the northwest of the island shown in Figure 4a (latitude/longitude location: 18.3,-67.0 to 18.4,-66.5)

388 is a feature of the topography and model structure, not data error. This area is dominated by karst hydrology



389 (Hughes and Schulz, 2020). Therefore, these areas of pooled water would likely not feature if karst processes
390 were explicitly represented in the model set up. The inclusion of karst processes was beyond the scope of this
391 study, and as this area is sparsely populated it is unlikely to impact the estimates of population exposure
392 presented.

393

394 **3.3 Characterising Changes in Population Exposure Under Present Day, 1.5°C and 2°C**

395 This research estimates changes in population exposure to hurricane rainfall-driven flooding for the island of
396 Puerto Rico under present day, 1.5°C and 2°C climate change. The climate change scenarios are analysed for
397 each individual climate model, as opposed to the aggregate results, as there are important differences between
398 models that are obscured when using the mean. This is a way of investigating uncertainty explicitly, by
399 understanding the differences between models. Studies such as Daron et al., (2021) have highlighted the
400 importance of assessing individual model performance when climate models give a wide range of projections.

401

402 Figure 5 shows the return period of a given exceedance of population exposure from hurricane rainfall-driven
403 flooding in Puerto Rico under present day, 1.5°C and 2°C climate change. Return periods of population
404 exposure exceedance above the 30-year return period are not considered and are thus faded in Figure 5. The
405 number of samples for each climate model scenario above the 30-year return period is too small (mean: 12.7
406 samples) to determine accurate estimates of population exposure above the 30-year return period (see Figure 5).
407 Thus, changes in population exposure above the 30-year return period in this event set are subject to significant
408 uncertainty resulting from limited samples at these event magnitudes and are therefore not considered further in
409 this analysis. A much longer event set would be required to simulate robust changes in population exposure at
410 higher magnitude return periods.

411

412 Three of the four climate models show agreement in the direction of change between present and future climate
413 change, with increases in population exposure associated with a given return period at 1.5°C and 2°C compared
414 to present day. However, one climate model (CanAM4) shows the opposite trend above the 10-year return
415 period (see Figure 6). One key reason for this is likely to be the differences in resolution of the underlying
416 Global Climate Model (GCM) data: CanAM4 GCM has a coarser resolution (2.81°x2.81°) than the next most
417 coarse GCM ECHAM6-3-LR (1.88°x1.88°). As a result, the underlying variables driving extreme hurricane
418 rainfall are less likely to be well-represented in CanAM4 compared to the other three climate models. It is well
419 understood that higher-resolution GCMs are better able to simulate the underlying conditions important for the
420 development of extreme rainfall and tropical cyclones (Knutson et al., 2020).

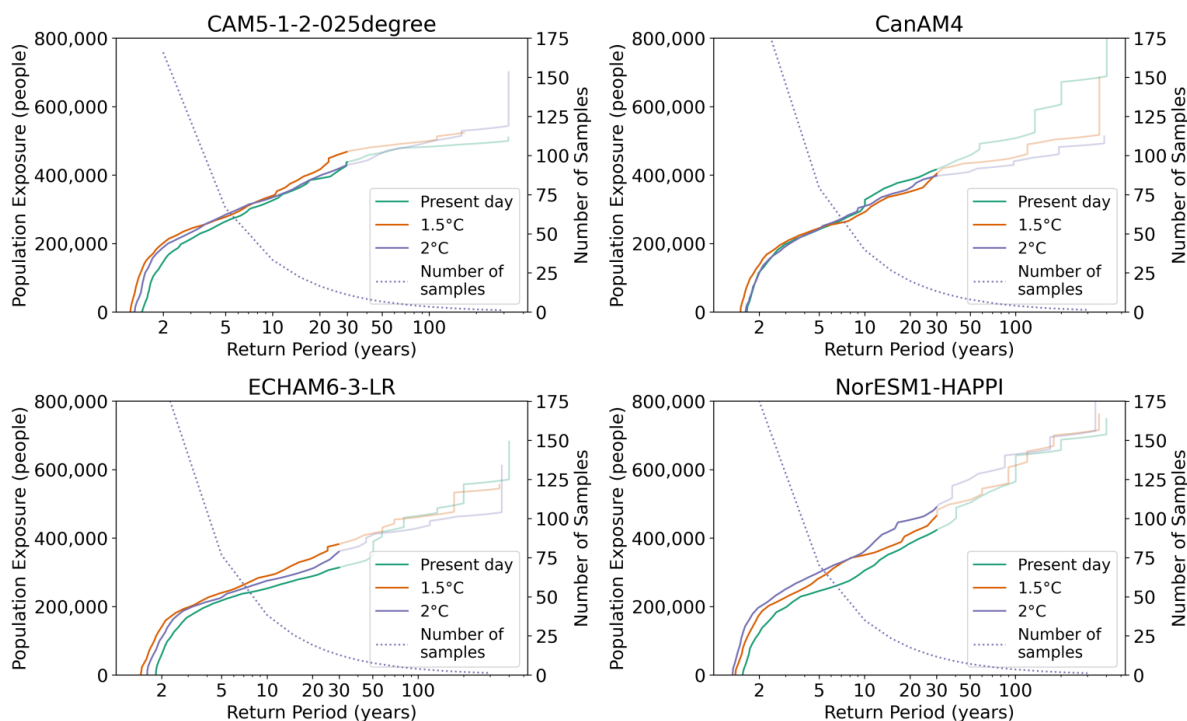


Figure 5 - Graph showing population exposure exceedance for present day, 1.5°C and 2°C climate change, as well as the number of samples in each climate model at a given return period (dotted line). Population exposure above the 30-year return period is faded to represent the uncertainty associated with the limited number of samples at these return periods.

421

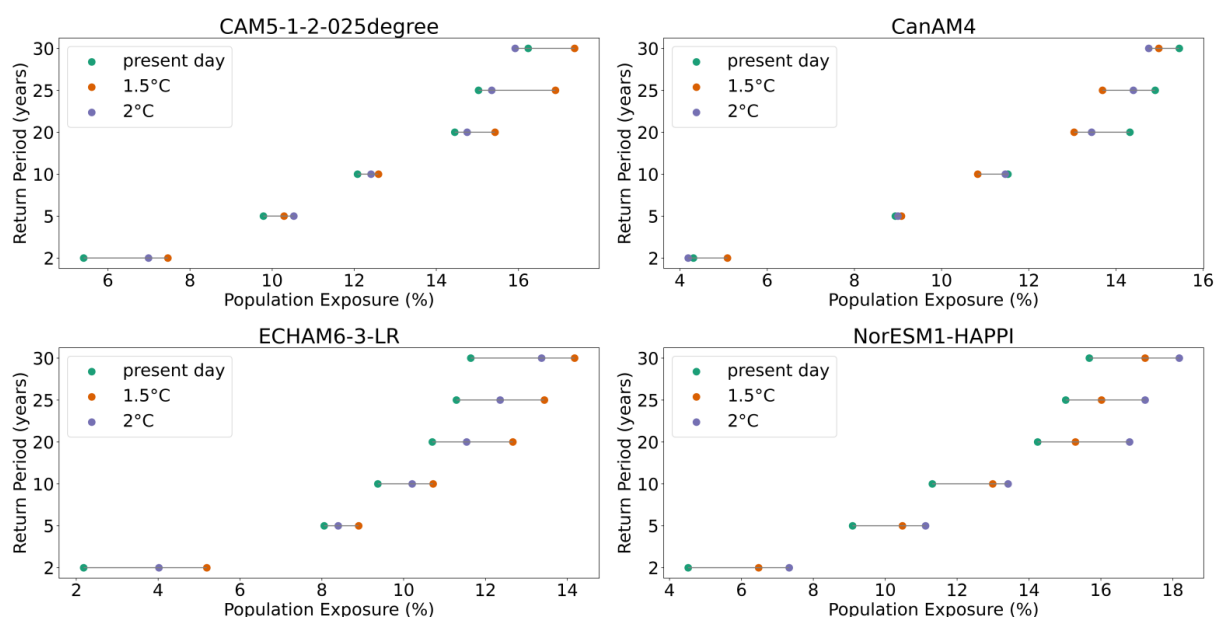
422 Present day population exposure to flooding from hurricane rainfall in Puerto Rico is approximately 2-5% at the
 423 two-year return period, rising to 8-10% at the five-year, 9-12% at the ten-year and 11-14% at the twenty-year
 424 return periods respectively (see Figure 5). These are the first published estimates of present day population
 425 exposure from flooding in Puerto Rico. It is difficult to corroborate population exposure estimates with those for
 426 previous events in Puerto Rico due to a lack of data, however these estimates are plausible given the universal
 427 island-wide flash flood warning given to Puerto Rico during Hurricane Maria (Pasch et al., 2018).

428

429 As shown in Figure 6, the estimated number of people exposed to flooding from hurricane rainfall on average
 430 every two years would increase by the largest percentage across the different return periods (20-140% at 1.5°C;
 431 -3-85% at 2°). The lower bound here represents the results from the CanAM4 model, which has the lowest
 432 GCM resolution. The reason for the widest range at the two-year return period could be because of the different
 433 bed elevations sized at the historical two-year return period for each climate model. For a return period
 434 population exposure of five years as shown in Figure 7, the percentage increase in population exposure at 1.5°C
 435 and 2°C ranges from 2-15% and 1-20%, respectively. This is a considerably lower range than the population
 436 exposure exceedance at the two-year return period, but also shows more agreement between the climate models.



437 As shown in Figure 6 there is a notable difference in population exposure exceedance between present day and
 438 1.5°C in three of the four climate models, but a less clear difference between 1.5°C and 2°C. In two of the four
 439 climate models (CAM5-1-2-025degree and ECHAM6-3-LR), the percentage of population exposed at a given
 440 return period is higher at 1.5°C compared to 2°C, and in one climate model (NorESM1-HAPPI), higher at 2°C
 441 compared to 1.5°C. In the CanAM4 climate model, depending on the return period, the percentage of population
 442 exposure varies between the three climate scenarios, and no consistent pattern is shown between the three across
 443 different return periods.
 444
 445



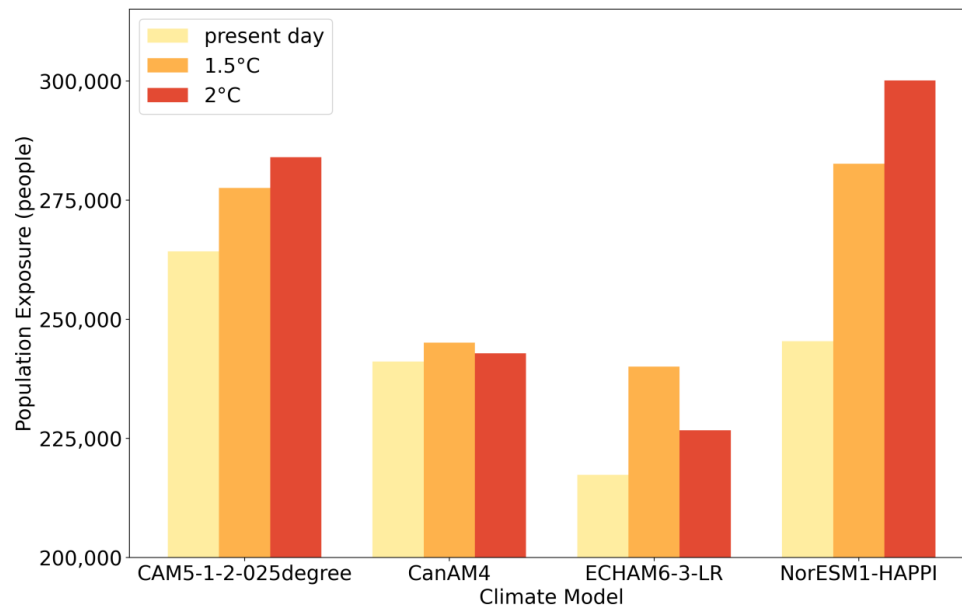
446

Figure 6 - Plot showing the percentage of population exposed to flooding under present day, 1.5°C and 2°C climate change, and the difference between the three scenarios for each HAPPI climate model. The green dot represents present day population exposure (as a percentage of the total population), with the orange and purple dots representing the population exposure (%) at 1.5°C and 2°C. The difference between the population exposure between the different scenarios is represented by the line between the dots.

447 Figure 7 demonstrates that the range in absolute population exposure numbers estimated for a given return
 448 period between the four climate models is the same as or greater than the percentage uplift in population
 449 exposure associated with 1.5°C and 2°C, highlighting the range of possible absolute population exposure
 450 estimates. For the 5-year return period, present day absolute population exposure ranges from 217,000
 451 (ECHAM6-3-LR) to 264,000 (CAM5-1-2-025degree). This is a 21% difference, whereas the highest population
 452 exposure increase is 22% between present day and 2°C for the NorESM1-HAPPI climate model. This
 453 underlines the difficulty in estimating current population exposure to flooding. This is not only the case in data-
 454 sparse areas such as Puerto Rico, but also in data-rich areas such as the conterminous US (Bates et al., 2021).
 455 However, the direction of change between the ‘present day’ and ‘future’ climate change (1.5°C and 2°C) is



456 robust across three of the four climate models, meaning the signal in population exposure to flooding is
457 observable when comparing present day and future climate change, despite the uncertainty in absolute terms.
458



459
460 **Figure 7 - Bar graph showing the number of people exposed to flooding under present day, 1.5°C and 2°C climate**
461 **change for the 5-year population exposure exceedance for each HAPPI climate model.**



462 **4 Discussion**

463 Our estimates of flood hazard and population exposure driven by hurricane rainfall under current and future climate
464 change supersedes previous efforts to estimate hurricane rainfall-driven flood risk in Puerto Rico. Previous estimates
465 rely on local-scale FEMA fluvial assessments or the global large-scale assessments that most often neglect small
466 islands through choice of scale. Although, the FEMA models will likely be more accurate locally where they exist,
467 depending on the local river channel and flood defence information that was available to the model developers. This
468 research is one of the first known published studies which propagates spatially and temporally explicit hurricane
469 rainfall through to the impact modelling of flood hazard and population exposure estimates, and the first in a small
470 island. Utilising hydrodynamic flood models to understand changes in flooding under climate change is a critical
471 gap in the literature, despite the widespread use of hydrodynamic models to assess current flood risk. The latest
472 IPCC AR6 Working Group I report demonstrated that changes in rainfall were still the dominant method used to
473 assess changes in pluvial flooding under climate change (Seneviratne et al., 2021). However, here we find that the
474 changes in population exposure between present day and 1.5°C and 2°C climate change do not correspond linearly
475 with changes in hurricane rainfall using the HAPPI climate models (Vosper et al., 2020) analysed here, and
476 therefore this rainfall proxy method may not be appropriate when investigating changes in flooding from hurricane
477 rainfall.

478 **4.1 Validating an Event-Based Model**

479 We present the first estimates of rainfall-driven flooding from Hurricane Maria using IMERG and NCEP Stage IV
480 precipitation data. Comparison against HWM data from Hurricane Maria showed that the RMSE of these estimates
481 was reasonable given the typical uncertainties in data of this type (IMERG: 1.18m, NCEP Stage IV: 1.22m). There
482 is uncertainty associated with the HWM vertical datum transformation using VDatum (+/-0.92m) which is likely to
483 impact the RMSE. However, these RMSEs have a similar magnitude to studies conducted in data-rich regions with
484 similar quality HWM data, such as the conterminous US (~1m) (Wing et al., 2021). This demonstrates that the
485 model is capable of realistically simulating flood depths, and thus the suitability of the model for estimating flood
486 hazard under current and future climate change. Inevitably, this finding should be considered alongside the inherent
487 limitations when comparing flood estimates to High Water Mark data. For example, RMSEs in this study are higher
488 than in studies such as Neal et al., (2009) (RMSE: 0.28m). Yet, the HWM data in this study is arguably lower
489 quality data due to the catastrophic nature of the hurricane which limited accessibility for post-event assessment due
490 to wide scale infrastructure failure (Main et al., 2021). HWMs in this study are concentrated in populated areas, and
491 were probably constrained to where it was safe to travel immediately post-event. The performance of the model is
492 likely biased towards these coastal, more populated areas. However, this is also where a considerable portion of the
493 risk is on the island, as this is where the majority of the population resides. Moreover, there are limitations of the
494 observation precipitation datasets used, which propagate into the flood estimates. For example, IMERG is likely to
495 underestimate orographic rainfall, which could explain why the flood extent using IMERG is lower than using
496 NCEP Stage IV (see Figure 2). This provides an incentive for the event set approach outlined in this study, as it



497 allows a consideration of a wider range of plausible events to get a greater understanding of uncertainty than just the
498 observed.

499

500 Based on the events selected as Hurricane Maria-like highlighted in Figure 3, we find that our event set contains
501 those like Hurricane Maria, and that these events have amongst the lowest RMSE in comparison to observed HWMs
502 from Hurricane Maria (range: 1.13-1.33m). It was expected that given the extreme magnitude of Hurricane Maria
503 (~115 year return period hurricane rainfall event: (Keellings and Hernández Ayala, 2019)), there would be a limited
504 number of events in our event set with this magnitude due to the comparatively short, simulated time record of our
505 event set (range: 332-427 years per climate model scenario). In our event set across all climate model scenarios, we
506 find 20 events that we classify as Hurricane Maria-like based on maximum total rainfall and spatial characteristics.
507 This finding firstly reinforces just how extreme Hurricane Maria was, following both the devastating impact on the
508 population and infrastructure (Audi et al., 2018; Michaud and Kates, 2017; Main et al., 2021), as well as the
509 literature examining the event in the context of the historical record (Keellings and Hernández Ayala, 2019; Ramos-
510 Scharrón and Arima, 2019). This also indicates that the model has the capacity to replicate events such as Hurricane
511 Maria when both maximum total rainfall and spatial characteristics are considered. Two key conclusions can be
512 taken from this. Firstly, this highlights the importance of variables other than rainfall when estimating rainfall-
513 driven flooding, such as spatial characteristics of the hurricane including landfall location and trajectory. Just
514 considering the rainfall was not sufficient to identify Maria-like events. As a result, simulating the spatial and
515 temporal distribution of the rainfall in an event set is a crucial step needed to accurately represent the relationship
516 between hurricane rainfall and flood hazard in Puerto Rico. This finding reinforces previous research which
517 identifies the importance of hurricane landfall and spatial location on the generation of floods in Puerto Rico
518 (Hernández Ayala et al., 2017; Hernández Ayala & Matyas, 2016; Smith et al., 2005). Secondly, considering there is
519 uncertainty in so-called observed flooding from Hurricane Maria (see Figure 2), the event set provides the
520 opportunity to assess many more realisations of events with similar characteristics to Hurricane Maria than available
521 just using observations. This may allow a better understanding of uncertainty in rainfall-driven flooding for a given
522 event, and thus a greater understanding of risk. Future research investigating changes in flooding from hurricane
523 rainfall should thus take an event-based approach as outlined in this study.

524 **4.2 Current Population Exposure to Flooding from Hurricane Rainfall**

525 Our results highlight the first published estimates of population exposure to flooding in Puerto Rico under the
526 present day climate, with approximately 8-10% of the population currently exposed to flooding from hurricane
527 rainfall at the five year recurrence interval. This level of population exposure has important implications for
528 resilience to floods. It also underlines the exposure to hydrometeorological hazards already experienced in SIDS,
529 which is a key reason for their high risk to climate change and disasters (Thomas et al., 2020). It is also worth noting
530 that these population exposure estimates are for the present day (2005-2016) climate at around 0.9°C of global mean
531 warming and therefore do not represent a pre-industrial climate. This means population exposure estimates for the
532 present day identified in this study are likely to be already influenced by climate change, given the significant



533 impact of climate change found on recent hurricane rainfall events in Puerto Rico such as Hurricane Maria
534 (Keellings and Hernández Ayala, 2019; Patricola and Wehner, 2018).

535 **4.3 Population Exposure to Flooding from Hurricane Rainfall Under 1.5°C and 2°C Climate Change**

536 The results presented in this research estimate that population exposure to flooding from hurricane rainfall will be
537 amplified under 1.5°C and 2°C in all but one of the four HAPPI climate models analysed. The Paris Agreement
538 includes the 1.5°C target as the higher ambition goal and is often touted as our best chance to limit the impacts of
539 climate change to within a ‘safe limit’. However, our analysis contributes to the discourse SIDS have been
540 highlighting for some time now, which is that even a 1.5°C temperature rise above preindustrial levels leads to a
541 serious threat to the adaptive capacity (Ourbak and Magnan, 2018; Mycoo, 2018; Hoegh-Guldberg et al., 2018;
542 Mycoo et al., 2022). Here, we find that even at 1.5°C, the increase in population exposure associated with hurricane
543 rainfall-driven flooding in Puerto Rico is enhanced for events with a return period below 30 years. This may have
544 wide-reaching implications for the resilience of Puerto Rico’s population. Moreover, although the 1.5°C goal is
545 technically feasible (IPCC, 2018, 2021), it is not currently the most likely temperature rise based on existing policy
546 pledges. At the time of writing, global temperature increase has already reached ~1.1°C above pre-industrial levels
547 (World Meteorological Organization, 2021). Based on our analysis, it is likely that flood hazard and population
548 exposure would increase further still under higher warming scenarios. These changes are likely to vary between
549 GCMs.

550
551 Due to the range in both absolute population numbers and the relative changes in population exposure between
552 present day, 1.5°C and 2°C across the four climate models in this event set, there is uncertainty in both how many
553 people might be exposed to a particular flood event, as well as how much this may change in the future. Moreover,
554 the range of present day absolute population numbers is often larger than the climate signal, which underlines the
555 difficulty in understanding current population exposure (Bates et al., 2021). This demonstrates the importance in
556 assessing a range of different climate model projections to understand the range of uncertainties, which taking an
557 event set approach enables because it allows many more realisations of a given event magnitude than is likely to
558 have occurred in the historical record to be considered. Overall, three of the four climate models utilized in this
559 study show that there is a difference in the percentage of the population exposed at a given return period under
560 1.5°C or 2°C climate change in comparison to present day. It is likely that the difference between 1.5°C and 2°C is
561 too small to determine a robust directional change above variability, particularly as only four of the >50 HAPPI
562 ensemble members are utilised in this analysis. Other studies have also shown a spread around the median in
563 precipitation, flood hazard and population exposure estimates under future scenarios (Bates et al., 2021; Swain et al.,
564 2020; Lopez-Cantu et al., 2020), as well as uncertain differences between 1.5°C and 2°C given the influence of
565 underlying uncertainty in the GCM and precipitation data (Uhe et al., 2019).

566
567 Other reasons for uncertainty in absolute population exposures likely stems from the choice of population data, and
568 the corresponding methodology used to assign population to pixels, as well as the underlying population data used to
569 inform the population totals. This is evidenced by the differences in total population between WorldPop, HRSL and



570 HRPDM as discussed in Section 2.3. Moreover, flood defences are not included in the model due to a lack of
571 available data, meaning the absolute population exposure numbers – particularly for the lower return periods where
572 flood defences are most likely to provide protection – will probably be an overestimate in some locations. If flood
573 defence information were available, the standards of protection could be applied to the exposure estimates provided
574 in this dataset to estimate population exposure when flood defences are included.

575 **4.4 Limitations of Event Set Size**

576 Population exposure estimates above the 30-year return period are subject to significant uncertainty due to the
577 limited number of samples (mean of <12.7 samples across the four climate models) available in the event set with
578 these return periods. As a result, the changes in population exposure between current, 1.5°C and 2°C above the 30-
579 year return period were not considered in this study. This was an acceptable trade off based on this current work, as
580 this study was most focused on understanding changes in lower magnitude, higher frequency events. Flood events
581 >30-year return period are often valley-filling, and therefore the impact of such events is already likely to be very
582 significant for the population, as demonstrated during Hurricane Maria (Pasch et al., 2018). Larger events also often
583 lead to a greater domestic and international response. However, smaller more frequent events lead to the erosion of
584 resilience in communities over time, and do not receive the same level of relief or response (Hamdan, 2015; Bull-
585 Kamanga et al., 2003; Allen et al., 2017; United Nations Office for Disaster Risk Reduction, 2019). Research to date
586 has also mostly focused on changes in the 100-year return period event (Arnell and Gosling, 2016; Lehner et al.,
587 2006; Hirabayashi et al., 2013). Therefore, assessing changes in lower magnitude, higher frequency events was a
588 key aim of this study. To detect changes in the 100-year return period population exposure, a much longer event set
589 would be required to detect a significant change between 1.5°C and 2°C. Although we have shown that 20 events
590 like Hurricane Maria do occur in the event set overall, preferably there would be at least 30-50 events to have
591 confidence in relative changes, as is shown in Figure 5. This would require at least 1000 years of synthetic data per
592 climate model as a minimum. This should be considered in the future when producing event sets derived from
593 GCMs with the intention to utilise these in flood impact modelling. Inevitably, running a much larger ensemble
594 comes at the expense of computational cost, therefore a trade-off, particularly with inundation model resolution, is
595 likely to be necessary.

596 **5 Conclusion**

597 We present the most detailed estimates of present day and future (1.5°C and 2°C) hurricane rainfall-driven flood
598 hazard and population exposure estimates in Puerto Rico to date. This analysis quantifies present day population
599 exposure to flooding in Puerto Rico for small to medium sized events (<30-year return period). Population exposure
600 to flooding is likely to increase under both 1.5°C and 2°C climate change. Estimates here suggest that for the present
601 day 8-10% of the total population of Puerto Rico would be exposed to flooding (defined as residing at a location
602 with inundation depth > 10cm) from hurricane rainfall every 5 years, increasing by 2-15% and 1-20% at 1.5°C and
603 2°C, respectively. Increases in the number of people exposed to small to medium sized flood events (<30-year return
604 period) could have a cumulative negative impact on the long-term resilience of the Puerto Rican population without
605 appropriate adaptation. Uncertainty in absolute population exposure estimates, as well as the range in estimated



606 percentage increases in flooding under 1.5°C and 2°C should be considered when using these estimates to inform
607 appropriate adaptation.

608

609 Through validation of our model in comparison with observed high water mark data for Hurricane Maria (~115-year
610 return period rainfall event), we find that our model is able to replicate similar levels of flooding to that which
611 occurred, and that there are events like Hurricane Maria in the event set when events with both similar maximum
612 total rainfall and spatial track characteristics are considered. This has important implications for future research, as
613 an event-based approach allows the assessment of many more plausible scenarios than is available in the observed
614 historical record.

615

616 Puerto Rico is predicted to experience increased population exposure to flooding associated with hurricane rainfall
617 in the future under 1.5°C and 2°C climate change. These findings add to the growing body of research that
618 highlights the critical and disproportionate risk climate change poses to Small Island Developing States, amidst the
619 uncomfortable irony that they have contributed amongst the least greenhouse gas emissions responsible for
620 anthropogenic climate change (Hoegh-Guldberg et al., 2018; Thomas et al., 2020). This highlights simultaneously
621 the impact of every increment of global temperature increase for Small Island Developing States and thus the
622 importance of high-ambition mitigation efforts, as well as the urgent need for increased climate change adaptation
623 and disaster risk reduction in the region.

624

625 **Data Availability**

626 The HAPPI climate model data described in Mitchell et al., (2017) doi:10.5194/gmd-10-571-2017 can be found and
627 downloaded under a Attribution-NonCommercial-ShareAlike 2.0 Generic License at:

628 https://www.happimip.org/happi_data/

629 The LiDAR data can be found on the USGS Data Access Viewer:

630 <https://coast.noaa.gov/dataviewer/#/lidar/search/where:ID=8630>

631 The LISFLOOD-FP hydraulic engine is available to download at: LISFLOOD-FP Developers. (2020). LISFLOOD-
632 FP 8.0 hydrodynamic model (Version 8.0). [Software]. Zenodo. <https://doi.org/10.5281/zenodo.4073011>

633 The WorldPop population data can be found at: Bondarenko et al., (2020) doi:10.5258/SOTON/WP00684 under a
634 Creative Commons Attribution 4.0 International License.

635 The High Water Mark data can be found on the USGS Flood Event Viewer:

636 <https://stn.wim.usgs.gov/FEV/#MariaSeptember2017>

637 IMERG data can be downloaded from the Global Precipitation Measurement database at:

638 <https://gpm.nasa.gov/data/imerg>

639 NCEP Stage IV data can be downloaded at: Du, J. 2011. NCEP/EMC 4KM Gridded Data (GRIB) Stage IV Data.

640 Version 1.0. UCAR/NCAR - Earth Observing Laboratory. <https://doi.org/10.5065/D6PG1QDD>

641 The probability of inundation and corresponding population exposure estimates maps are available via the data.bris
642 Research Data Repository (doi available at final publication).



643

644 **Author contribution**

645 LA conceptualized, conducted the analysis, methodology and validation and wrote the manuscript; JN and PDB
646 conceptualized, supervised and contributed to the analysis, methodology and validation; EV, DC and JS were
647 involved in the data curation and methodology; DM was involved in conceptualization. All authors were involved in
648 reviewing and editing the manuscript.

649

650 **Competing interests**

651 The authors declare that they have no conflict of interest.

652 **Acknowledgments**

653 Leanne Archer is supported by the UKRI NERC GW4+ Doctoral Training Partnership NE/S007504/1. Paul Bates is
654 supported by a Royal Society Wolfson Research Merit award. Jeffrey Neal is supported by UKRI NERC grants
655 NE/S003061/1 and NE/S006079/1. Emily Vosper is supported by the UKRI ERSFC Centre for Doctoral Training.

656

657 **References**

- 658 Aldridge, T., Gunawan, O., Moore, R. J., Cole, S. J., Boyce, G., and Cowling, R.: Developing an impact library for
659 forecasting surface water flood risk, *J Flood Risk Manag*, 13, <https://doi.org/10.1111/jfr3.12641>, 2020.
- 660 Allen, A., Zilbert Soto, L., Wesely, J., Belkow, T., Ferro, V., Lambert, R., Langdown, I., and Samanamú, A.: From
661 state agencies to ordinary citizens: reframing risk-mitigation investments and their impact to disrupt urban risk traps
662 in Lima, Peru, *Environ Urban*, 29, 477–502, <https://doi.org/10.1177/0956247817706061>, 2017.
- 663 Arnell, N. W. and Gosling, S. N.: The impacts of climate change on river flood risk at the global scale, *Clim
664 Change*, 134, 387–401, <https://doi.org/10.1007/S10584-014-1084-5>, 2016.
- 665 Audi, C., Segarra, L., Irwin, C., Craig, P., Skelton, C., and Bestul, N.: Ascertainment of the Estimated Excess
666 Mortality from Hurricane María in Puerto Rico, Washington D.C., 2018.
- 667 Barnes, R.: Parallel non-divergent flow accumulation for trillion cell digital elevation models on desktops or
668 clusters, *Environmental Modelling & Software*, 92, 202–212, <https://doi.org/10.1016/J.ENVSOFT.2017.02.022>,
669 2017.
- 670 Bates, P. D., Horritt, M. S., and Fewtrell, T. J.: A simple inertial formulation of the shallow water equations for
671 efficient two-dimensional flood inundation modelling, *J Hydrol (Amst)*, 387, 33–45,
672 <https://doi.org/10.1016/j.jhydrol.2010.03.027>, 2010.
- 673 Bates, P. D., Quinn, N., Sampson, C., Smith, A., Wing, O., Sosa, J., Savage, J., Olcese, G., Neal, J., Schumann, G.,
674 Giustarini, L., Coxon, G., Porter, J. R., Amodeo, M. F., Chu, Z., Lewis-Gruss, S., Freeman, N. B., Houser, T.,
675 Delgado, M., Hamidi, A., Bolliger, I., McCusker, K., Emanuel, K., Ferreira, C. M., Khalid, A., Haigh, I. D.,
676 Couasnon, A., Kopp, R., Hsiang, S., and Krajewski, W. F.: Combined modelling of US fluvial, pluvial and coastal
677 flood hazard under current and future climates, *Water Resour Res*, 57, <https://doi.org/10.1029/2020wr028673>, 2021.



- 678 Bates, P. D., Savage, J., Wing, O., Quinn, N., Sampson, C., Neal, J., and Smith, A.: A climate-conditioned
679 catastrophe risk model for UK flooding, *Natural Hazards and Earth System Sciences*, 23, 891–908,
680 <https://doi.org/10.5194/NHESS-23-891-2023>, 2023.
- 681 Bernet, D. B., Zischg, A. P., Prasuhn, V., and Weingartner, R.: Modeling the extent of surface water floods in rural
682 areas: Lessons learned from the application of various uncalibrated models, *Environmental Modelling and Software*,
683 109, 134–151, <https://doi.org/10.1016/j.envsoft.2018.08.005>, 2018.
- 684 Bernet, D. B., Trefalt, S., Martius, O., Weingartner, R., Mosimann, M., Röthlisberger, V., and Zischg, A. P.:
685 Characterizing precipitation events leading to surface water flood damage over large regions of complex terrain,
686 *Environmental Research Letters*, 14, <https://doi.org/10.1088/1748-9326/ab127c>, 2019.
- 687 Blanc, J., Hall, J. W., Roche, N., Dawson, R. J., Cesses, Y., Burton, A., and Kilsby, C. G.: Enhanced efficiency of
688 pluvial flood risk estimation in urban areas using spatial-temporal rainfall simulations, *J Flood Risk Manag*, 5, 143–
689 152, <https://doi.org/10.1111/j.1753-318X.2012.01135.x>, 2012.
- 690 Mapping the world to help aid workers, with weakly, semi-supervised learning:
691 <https://ai.facebook.com/blog/mapping-the-world-to-help-aid-workers-with-weakly-semi-supervised-learning>, last
692 access: 1 June 2020.
- 693 Bondarenko, M., Kerr, D., Sorichetta, A., and Tatem, A. J.: Census/projection-disaggregated gridded population
694 datasets for 189 countries in 2020 using Built-Settlement Growth Model (BSGM) outputs, WorldPop, University of
695 Southampton, Southampton, <https://doi.org/10.5258/SOTON/WP00684>, 2020.
- 696 Bull-Kamanga, L., Diagne, K., Lavell, A., Leon, E., Lerise, F., MacGregor, H., Maskrey, A., Meshack, M., Pelling,
697 M., Reid, H., Satterthwaite, D., Songsore, J., Westgate, K., and Yitambe, A.: From everyday hazards to disasters: the
698 accumulation of risk in urban areas, *Environ Urban*, 15, 193–204, <https://doi.org/10.1177/095624780301500109>,
699 2003.
- 700 Burgess, C. P., Taylor, M. A., Stephenson, T., Mandal, A., and Powell, L.: A macro-scale flood risk model for
701 Jamaica with impact of climate variability, *Natural Hazards*, 78, 231–256, [https://doi.org/10.1007/s11069-015-1712-](https://doi.org/10.1007/s11069-015-1712-z)
702 [z](https://doi.org/10.1007/s11069-015-1712-z), 2015.
- 703 Caban, P.: Hurricane Maria’s Aftermath: Redefining Puerto Rico’s Colonial Status, *Current History*, 118, 43–49,
704 2019.
- 705 Czajkowski, J., Villarini, G., Montgomery, M., Michel-Kerjan, E., and Goska, R.: Assessing Current and Future
706 Freshwater Flood Risk from North Atlantic Tropical Cyclones via Insurance Claims, *Sci Rep*, 7, 1–10,
707 <https://doi.org/10.1038/srep41609>, 2017.
- 708 Daron, J., Lorenz, S., Taylor, A., and Dessai, S.: Communicating future climate projections of precipitation change,
709 *Clim Change*, 166, 1–20, <https://doi.org/10.1007/S10584-021-03118-9/FIGURES/5>, 2021.
- 710 Dinku, T., Chidzambwa, S., Ceccato, P., Connor, S. J., and Ropelewski, C. F.: Validation of high-resolution satellite
711 rainfall products over complex terrain, <http://dx.doi.org/10.1080/01431160701772526>, 29, 4097–4110,
712 <https://doi.org/10.1080/01431160701772526>, 2008.
- 713 NCEP/EMC 4KM Gridded Data (GRIB) Stage IV Data:



- 714 Emanuel, K. and Jagger, T.: On Estimating Hurricane Return Periods, *J Appl Meteorol Climatol*, 49, 837–844,
715 <https://doi.org/10.1175/2009JAMC2236.1>, 2010.
- 716 Falconer, R. H., Cobby, D., Smyth, P., Astle, G., Dent, J., and Golding, B.: Pluvial flooding: new approaches in
717 flood warning, mapping and risk management, *J Flood Risk Manag*, 2, 198–208, [https://doi.org/10.1111/j.1753-](https://doi.org/10.1111/j.1753-318X.2009.01034.x)
718 [318X.2009.01034.x](https://doi.org/10.1111/j.1753-318X.2009.01034.x), 2009.
- 719 Feldmann, M., Emanuel, K., Zhu, L., and Lohmann, U.: Estimation of Atlantic Tropical Cyclone Rainfall Frequency
720 in the United States, *J Appl Meteorol Climatol*, 58, 1853–1866, <https://doi.org/10.1175/JAMC-D-19-0011.1>, 2019.
- 721 Guerreiro, S. B., Glenis, V., Dawson, R. J., and Kilsby, C.: Pluvial flooding in European cities-A continental
722 approach to urban flood modelling, *Water (Switzerland)*, 9, <https://doi.org/10.3390/w9040296>, 2017.
- 723 Hall, J.: Direct Rainfall Flood Modelling: The Good, the Bad and the Ugly, *Australasian Journal of Water*
724 *Resources*, 19, 74–85, <https://doi.org/10.7158/13241583.2015.11465458>, 2015.
- 725 Hamdan, F.: Intensive and extensive disaster risk drivers and interactions with recent trends in the global political
726 economy, with special emphasis on rentier states, *International Journal of Disaster Risk Reduction*, 14, 273–289,
727 <https://doi.org/10.1016/j.ijdrr.2014.09.004>, 2015.
- 728 Hankin, B., Waller, S., Astle, G., and Kellagher, R.: Mapping space for water: screening for urban flash flooding, *J*
729 *Flood Risk Manag*, 1, 13–22, <https://doi.org/10.1111/j.1753-318x.2008.00003.x>, 2008.
- 730 Hawker, L., Bates, P. D., Neal, J., and Rougier, J.: Perspectives on Digital Elevation Model (DEM) Simulation for
731 Flood Modeling in the Absence of a High-Accuracy Open Access Global DEM, *Front Earth Sci (Lausanne)*, 6,
732 <https://doi.org/10.3389/feart.2018.00233>, 2018.
- 733 Hernández Ayala, J. J. and Matyas, C. J.: Tropical cyclone rainfall over Puerto Rico and its relations to
734 environmental and storm-specific factors, *International Journal of Climatology*, 36, 2223–2237,
735 <https://doi.org/10.1002/joc.4490>, 2016.
- 736 Hernández Ayala, J. J., Keellings, D., Waylen, P. R., and Matyas, C. J.: Extreme floods and their relationship with
737 tropical cyclones in Puerto Rico, *Hydrological Sciences Journal*, 62, 2103–2119,
738 <https://doi.org/10.1080/02626667.2017.1368521>, 2017.
- 739 Hirabayashi, Y., Mahendran, R., Koirala, S., Konoshima, L., Yamazaki, D., Watanabe, S., Kim, H., and Kanae, S.:
740 Global flood risk under climate change, *Nat Clim Chang*, 3, 816–821, <https://doi.org/10.1038/nclimate1911>, 2013.
- 741 Hoegh-Guldberg, O., Jacob, D., Taylor, M., Bindi, M., Brown, S., Camilloni, I., Diedhiou, A., and Djalante, R.:
742 Chapter 3: Impacts of 1.5°C global warming on natural and human systems, in: *Global warming of 1.5°C. An IPCC*
743 *Special Report on the impacts of global warming of 1.5°C above pre-industrial levels and related global greenhouse*
744 *gas emission pathways, in the context of strengthening the global response to the threat of climate change*, edited by:
745 Intergovernmental Panel on Climate Change, Intergovernmental Panel on Climate Change, Geneva, 175–311, 2018.
- 746 Hughes, K. S. and Schulz, W. H.: Map Depicting Susceptibility to Landslides Triggered by Intense Rainfall. Open-
747 File Report 2020–1022, Denver, <https://doi.org/https://doi.org/10.3133/ofr20201022>., 2020.
- 748 IPCC: Summary for Policymakers, in: *Global Warming of 1.5°C. An IPCC Special Report on the impacts of global*
749 *warming of 1.5°C above pre-industrial levels and related global greenhouse gas emission pathways, in the context of*
750 *strengthening the global response to the threat of climate change*, edited by: Masson-Delmotte, V., Zhai, P., Pörtner,



- 751 H.-O., Roberts, D., Skea, J., Shukla, P. R., Pirani, A., Moufouma-Okia, W., Péan, C., Pidcock, R., Connors, S.,
752 Matthews, J. B. R., Chen, Y., Zhou, X., Gomis, M. I., Lonnoy, E., Maycock, T., Tignor, M., and Waterfield, T.,
753 Cambridge University Press, Cambridge, 1–24, 2018.
- 754 IPCC: Summary for Policymakers, in: Climate Change 2021: The Physical Science Basis. Contribution of Working
755 Group I to the Sixth Assessment Report of the Intergovernmental Panel on Climate Change, edited by: Masson-
756 Delmotte, V., Zhai, P., Pirani, A., Connors, S. L., Péan, C., Berger, S., Caud, N., Chen, Y., Goldfarb, L., Gomis, M.
757 I., Huang, M., Leitzell, K., Lonnoy, E., Matthews, J. B. R., Maycock, T. K., Waterfield, T., Yelekçi, O., Yu, R., and
758 Zhou, B., Cambridge University Press, Cambridge, 2021.
- 759 Jetten, V.: CHaRIM Project St Vincent National Flood Hazard Map Methodology and Validation Report, Enschede,
760 The Netherlands, 2016.
- 761 Jiménez Cisneros, B. E., Oki, T., Arnell, N. W., Benito, G., Cogley, J. G., Döll, P., Jiang, T., and Mwakilila, S. S.:
762 Freshwater Resources, in: Climate Change 2014: Impacts, Adaptation, and Vulnerability. Part A: Global and Sectoral
763 Aspects. Contribution of Working Group II to the Fifth Assessment Report of the Intergovernmental Panel on
764 Climate Change, edited by: Field, C. B., Barros, V. R., Dokken, D. J., Mach, K. J., Mastrandrea, M. D., Bilir, T. E.,
765 Chatterjee, M., Ebi, K. L., Estrada, Y. O., Genova, R. C., Girma, B., Kissel, E. S., Levy, A. N., MacCracken, S.,
766 Mastrandrea, P. R., and L.L.White, Cambridge University Press, Cambridge, 2014.
- 767 Joyette, A. R. T., Nurse, L. A., and Pulwarty, R. S.: Disaster risk insurance and catastrophe models in risk-prone
768 small Caribbean islands, *Disasters*, 39, 467–492, <https://doi.org/10.1111/disa.12118>, 2014.
- 769 Keellings, D. and Hernández Ayala, J. J.: Extreme Rainfall Associated With Hurricane Maria Over Puerto Rico and
770 Its Connections to Climate Variability and Change, *Geophys Res Lett*, 46, 2964–2973,
771 <https://doi.org/10.1029/2019GL082077>, 2019.
- 772 Knutson, T., Camargo, S. J., Chan, J. C. L., Emanuel, K., Ho, C.-H., Kossin, J., Mohapatra, M., Satoh, M., Sugi, M.,
773 Walsh, K., and Wu, L.: Tropical Cyclones and Climate Change Assessment: Part II. Projected Response to
774 Anthropogenic Warming, *Bull Am Meteorol Soc*, 101, E303–E322, <https://doi.org/10.1175/bams-d-18-0194.1>,
775 2020.
- 776 Kossin, J. P., Knapp, K. R., Olander, T. L., and Velden, C. S.: Global increase in major tropical cyclone exceedance
777 probability over the past four decades, *Proceedings of the National Academy of Sciences*, 117, 11975–11980,
778 <https://doi.org/10.1073/PNAS.1920849117>, 2020.
- 779 Lehner, B., Döll, P., Alcamo, J., Henrichs, T., and Kaspar, F.: Estimating the Impact of Global Change on Flood and
780 Drought Risks in Europe: A Continental, Integrated Analysis, *Clim Change*, 75, 273–299,
781 <https://doi.org/10.1007/S10584-006-6338-4>, 2006.
- 782 Leopold, L. B. and Maddock, T.: *The Hydraulic Geometry of Stream Channels and Some Physiographic*
783 *Implications*, Washington D.C., 1953.
- 784 Leyk, S., Gaughan, A. E., Adamo, S. B., De Sherbinin, A., Balk, D., Freire, S., Rose, A., Stevens, F. R.,
785 Blankespoor, B., Frye, C., Comenetz, J., Sorichetta, A., Macmanus, K., Pistolesi, L., Levy, M., Tatem, A. J., and
786 Pesaresi, M.: The spatial allocation of population: a review of large-scale gridded population data products and their
787 fitness for use, *Earth Syst Sci Data*, 11, 1385–1409, <https://doi.org/10.5194/essd-11-1385-2019>, 2019.



- 788 LISFLOOD-FP Developers: LISFLOOD-FP 8.0 hydrodynamic model (8.0),
789 <https://doi.org/https://doi.org/10.5281/zenodo.4073011>, 2020.
- 790 Lloyd, C. T., Sorichetta, A., and Tatem, A. J.: High resolution global gridded data for use in population studies, *Sci*
791 *Data*, 4, 1–17, <https://doi.org/10.1038/sdata.2017.1>, 2017.
- 792 Lopez-Cantu, T., Prein, A. F., and Samaras, C.: Uncertainties in Future U.S. Extreme Precipitation From
793 Downscaled Climate Projections, *Geophys Res Lett*, 47, <https://doi.org/10.1029/2019GL086797>, 2020.
- 794 Lu, P., Lin, N., Emanuel, K., Chavas, D., and Smith, J.: Assessing Hurricane Rainfall Mechanisms Using a Physics-
795 Based Model: Hurricanes Isabel (2003) and Irene (2011), *Journal of Atmospheric Sciences*, 75, 2337–2358,
796 <https://doi.org/10.1175/JAS-D-17-0264.1>, 2018.
- 797 Lumbroso, D., Boyce, S., Bast, H., and Walmsley, N.: The challenges of developing rainfall intensity-duration-
798 frequency curves and national flood hazard maps for the Caribbean, *The Journal of Flood Risk Management*, 4, 42–
799 52, 2011.
- 800 Main, J. A., Dillard, M., Kuligowski, E. D., Davis, B., Dukes, J., Harrison, K., Helgeson, J., Johnson, K., Levitan,
801 M., Mitrani-Reiser, J., Weaver, S., Yeo, D., Aponte-Bermúdez, L. D., Cline, J., Kirsch, T., and Ross, W. L.:
802 Learning from Hurricane Maria’s Impacts on Puerto Rico: A Progress Report, Washington D.C.,
803 <https://doi.org/10.6028/NIST.SP.1262>, 2021.
- 804 Mazzoleni, M., Mård, J., Rusca, M., Odongo, V., Lindersson, S., and Di Baldassarre, G.: Floodplains in the
805 Anthropocene: A global analysis of the interplay between human population, built environment and flood severity,
806 *Water Resour Res*, <https://doi.org/10.1029/2020WR027744>, 2020.
- 807 Mei, W. and Xie, S.-P.: Intensification of landfalling typhoons over the northwest Pacific since the late 1970s,
808 *Nature Geoscience* 2016 9:10, 9, 753–757, <https://doi.org/10.1038/ngeo2792>, 2016.
- 809 Michaud, J. and Kates, J.: Public Health in Puerto Rico after Hurricane Maria, San Francisco, 2017.
- 810 Mitchell, D., James, R., Forster, P. M., Betts, R. A., Shiogama, H., and Allen, M.: Realizing the impacts of a 1.5 °C
811 warmer world, *Nat Clim Chang*, 6, 735–737, <https://doi.org/10.1186/s40665-015-0010-z>, 2016.
- 812 Mitchell, D., Achutarao, K., Allen, M., Bethke, I., Beyerle, U., Ciavarella, A., Forster, P. M., Fuglestedt, J., Gillett,
813 N., Haustein, K., Ingram, W., Iversen, T., Kharin, V., Klingaman, N., Massey, N., Fischer, E., Schleussner, C.-F.,
814 Scinocca, J., Seland, Ø., Shiogama, H., Shuckburgh, E., Sparrow, S., Stone, D., Uhe, P., Wallom, D., Wehner, M.,
815 and Zaaboul, R.: Half a degree additional warming, prognosis and projected impacts (HAPPI): background and
816 experimental design, *Geosci. Model Dev*, 10, 571–583, <https://doi.org/10.5194/gmd-10-571-2017>, 2017.
- 817 Moftakhari, H. R., AghaKouchak, A., Sanders, B. F., and Matthew, R. A.: Cumulative hazard: The case of nuisance
818 flooding, *Earths Future*, 5, 214–223, <https://doi.org/10.1002/2016EF000494>, 2017.
- 819 Monioudi, I., Asariotis, R., Becker, A., Bhat, C., Dowding-Gooden, D., Esteban, M., Feyen, L., Mentaschi, L.,
820 Nikolaou, A., Nurse, L., Phillips, W., Smith, D., Satoh, M., Trotz, U. O., Velegrakis, A. F., Voukouvalas, E.,
821 Vousdoukas, M. I., and Witkop, R.: Climate change impacts on critical international transportation assets of
822 Caribbean Small Island Developing States (SIDS): the case of Jamaica and Saint Lucia, *Reg Environ Change*, 18,
823 2211–2225, <https://doi.org/10.1007/s10113-018-1360-4>, 2018.



- 824 Mycoo, M. A.: Beyond 1.5°C: vulnerabilities and adaptation strategies for Caribbean Small Island Developing
825 States, *Reg Environ Change*, 18, 2341–2353, <https://doi.org/10.1007/s10113-017-1248-8>, 2018.
- 826 Mycoo, M. A., Wairiu, M., Campbell, D., Duvat, V., Golbuu, Y., Maharaj, S., Nalau, J., Nunn, P., Pinnegar, J., and
827 Warrick, O.: Small Islands, in: *Climate Change 2022: Impacts, Adaptation and Vulnerability. Contribution of*
828 *Working Group II to the Sixth Assessment Report of the Intergovernmental Panel on Climate Change*, Cambridge
829 University Press, Cambridge, 2022.
- 830 IMERG: Integrated Multi-satellitE Retrievals for GPM | NASA Global Precipitation Measurement Mission:
831 <https://gpm.nasa.gov/data/imerg>, last access: 17 May 2023.
- 832 Major Hurricane Maria - September 20, 2017:
- 833 Neal, J., Bates, P. D., Fewtrell, T. J., Hunter, N. M., Wilson, M. D., and Horritt, M. S.: Distributed whole city water
834 level measurements from the Carlisle 2005 urban flood event and comparison with hydraulic model simulations, *J*
835 *Hydrol (Amst)*, 368, 42–55, <https://doi.org/10.1016/j.jhydrol.2009.01.026>, 2009.
- 836 Neal, J., Schumann, G., and Bates, P.: A subgrid channel model for simulating river hydraulics and floodplain
837 inundation over large and data sparse areas, *Water Resour Res*, 48, <https://doi.org/10.1029/2012WR012514>, 2012.
- 838 Neal, J., Hawker, L., Savage, J., Durand, M., Bates, P., and Sampson, C.: Estimating River Channel Bathymetry in
839 Large Scale Flood Inundation Models, *Water Resour Res*, 57, <https://doi.org/10.1029/2020wr028301>, 2021.
- 840 Nicholls, R. J., Brown, S., Goodwin, P., Wahl, T., Lowe, J., Solan, M., Godbold, J. A., Haigh, I. D., Lincke, D.,
841 Hinkel, J., Wolf, C., and Merken, J. L.: Stabilization of global temperature at 1.5°C and 2.0°C: Implications for
842 coastal areas, *Philosophical Transactions of the Royal Society A: Mathematical, Physical and Engineering Sciences*,
843 376, <https://doi.org/10.1098/rsta.2016.0448>, 2018.
- 844 Nurse, L. A., McLean, R. F., Agard Trinidad, J., Pascal Briguglio, L., Duvat-Magnan, V., Pelesikoti, N., Tompkins,
845 E., and Webb, A.: Small Islands, in: *Climate Change 2014: Impacts, Adaptation, and Vulnerability. Part B: Regional*
846 *Aspects. Contribution of Working Group II to the Fifth Assessment Report of the Intergovernmental Panel on*
847 *Climate Change*, edited by: Intergovernmental Panel on Climate Change, Cambridge, 1613–1654, 2014.
- 848 Nuswantoro, R., Diermanse, F., and Molkenhain, F.: Probabilistic flood hazard maps for Jakarta derived from a
849 stochastic rain-storm generator, *J Flood Risk Manag*, 9, 105–124, <https://doi.org/10.1111/jfr3.12114>, 2016.
- 850 Ourbak, T. and Magnan, A. K.: The Paris Agreement and climate change negotiations: Small Islands, big players,
851 <https://doi.org/10.1007/s10113-017-1247-9>, 1 December 2018.
- 852 Pasch, R. J., Penny, A. B., and Berg, R.: Hurricane Maria 16–30 September 2017, National Hurricane Center
853 Tropical Cyclone Report, National Hurricane Center, Miami, 2018.
- 854 Patricola, C. M. and Wehner, M. F.: Anthropogenic influences on major tropical cyclone events, *Nature*, 563, 339–
855 346, <https://doi.org/10.1038/s41586-018-0673-2>, 2018.
- 856 Pickup, G. and Warner, R. F.: Effects of hydrologic regime on magnitude and frequency of dominant discharge, *J*
857 *Hydrol (Amst)*, 29, 51–75, [https://doi.org/10.1016/0022-1694\(76\)90005-6](https://doi.org/10.1016/0022-1694(76)90005-6), 1976.
- 858 Pokhrel, R., Cos, S. del, Montoya Rincon, J. P., Glenn, E., and González, J. E.: Observation and modeling of
859 Hurricane Maria for damage assessment, *Weather Clim Extrem*, 33, 100331,
860 <https://doi.org/10.1016/J.WACE.2021.100331>, 2021.



- 861 Prato, R. A., Jetten, V., and Alkema, D.: Rural Flash-flood Behavior in Gouyave Watershed, Grenada,
862 Caribbean Island, *Geoplanning: Journal of Geomatics and Planning*, 3, 161,
863 <https://doi.org/10.14710/geoplanning.3.2.161-170>, 2016.
- 864 Ramos-Scharrón, C. E. and Arima, E.: Hurricane María's Precipitation Signature in Puerto Rico: A Conceivable
865 Presage of Rains to Come, *Sci Rep*, 9, <https://doi.org/10.1038/s41598-019-52198-2>, 2019.
- 866 Ranasinghe, R., Ruane, A. C., Vautard, R., Arnell, N., Coppola, E., Cruz, F. A., Dessai, S., Islam, A. S., Rahimi, M.,
867 Ruiz, D., Carrascal, Sillmann, J., Sylla, M. B., Tebaldi, C., Wang, W., and Zaaboul, R.: Climate Change Information
868 for Regional Impact and for Risk Assessment, in: *Climate Change 2021: The Physical Science Basis. Contribution*
869 *of Working Group I to the Sixth Assessment Report of the Intergovernmental Panel on Climate Change*, edited
870 by: Masson-Delmotte, V., Zhai, P., Pirani, A., Connors, S. L., Péan, C., Berger, S., Caud, N., Chen, Y., Goldfarb, L.,
871 Gomis, M. I., Huang, M., Leitzell, K., Lonnoy, E., Matthews, J. B. R., Maycock, T. K., Waterfield, T., Yelekçi, O.,
872 Yu, R., and Zhou, B., Cambridge University Press, Cambridge, 2021.
- 873 Rappaport, E. N.: Fatalities in the United States from Atlantic Tropical Cyclones: New Data and Interpretation, *Bull*
874 *Am Meteorol Soc*, 95, 341–346, <https://doi.org/10.1175/BAMS-D-12-00074.1>, 2014.
- 875 Rasmussen, D. J., Bittermann, K., Buchanan, M. K., Kulp, S., Strauss, B. H., Kopp, R. E., and Oppenheimer, M.:
876 Extreme sea level implications of 1.5 °C, 2.0 °C, and 2.5 °C temperature stabilization targets in the 21st and 22nd
877 centuries, *Environmental Research Letters*, 13, 034040, <https://doi.org/10.1088/1748-9326/AAAC87>, 2018.
- 878 Reed, F., Gaughan, A., Stevens, F., Yetman, G., Sorichetta, A., and Tatem, A.: Gridded Population Maps Informed
879 by Different Built Settlement Products, *Data (Basel)*, 3, 33, <https://doi.org/10.3390/data3030033>, 2018.
- 880 Rivera, D. Z.: Disaster Colonialism: A Commentary on Disasters beyond Singular Events to Structural Violence, *Int*
881 *J Urban Reg Res*, <https://doi.org/10.1111/1468-2427.12950>, 2020.
- 882 Rosenzweig, B. R., McPhillips, L., Chang, H., Cheng, C., Welty, C., Matsler, M., Iwaniec, D., and Davidson, C. I.:
883 Pluvial flood risk and opportunities for resilience, *WIREs Water*, 5, <https://doi.org/10.1002/wat2.1302>, 2018.
- 884 Rözer, V., Kreibich, H., Schröter, K., Müller, M., Sairam, N., Doss-Gollin, J., Lall, U., and Merz, B.: Probabilistic
885 Models Significantly Reduce Uncertainty in Hurricane Harvey Pluvial Flood Loss Estimates, *Earths Future*, 7, 384–
886 394, <https://doi.org/10.1029/2018EF001074>, 2019.
- 887 Sampson, C. C., Bates, P. D., Neal, J. C., and Horritt, M. S.: An automated routing methodology to enable direct
888 rainfall in high resolution shallow water models, *Hydrol Process*, 27, 467–476, <https://doi.org/10.1002/hyp.9515>,
889 2013.
- 890 Sampson, C. C., Smith, A. M., Bates, P. B., Neal, J. C., Alfieri, L., and Freer, J. E.: A high-resolution global flood
891 hazard model, *Water Resour Res*, 51, 7358–7381, <https://doi.org/10.1002/2015WR016954>, 2015.
- 892 Savage, J. T. S., Bates, P., Freer, J., Neal, J., and Aronica, G.: When does spatial resolution become spurious in
893 probabilistic flood inundation predictions?, *Hydrol Process*, 30, 2014–2032, <https://doi.org/10.1002/hyp.10749>,
894 2016.
- 895 Sayers, P. B., Horritt, M. S., Carr, S., Kay, A., Mauz, J., Lamb, R., and Penning-Rowsell, E.: Third UK Climate
896 Change Risk Assessment (CCRA3) Future flood risk Main Report Final Report prepared for the Committee on
897 Climate Change, UK, London, 2020.



- 898 Schaller, N., Sillmann, J., Müller, M., Haarsma, R., Hazeleger, W., Hegdahl, T. J., Kelder, T., van den Oord, G.,
899 Weerts, A., and Whan, K.: The role of spatial and temporal model resolution in a flood event storyline approach in
900 western Norway, *Weather Clim Extrem*, 29, <https://doi.org/10.1016/J.WACE.2020.100259>, 2020.
- 901 Seneviratne, S. I., Zhang, X., Adnan, M., Badi, W., Dereczynski, C., Luca, A. Di, Ghosh, S., Iskandar, I., Kossin, J.,
902 Lewis, S., Otto, F., Pinto, I., Satoh, M., Vicente-Serrano, S. M., Wehner, M., and B. Zhou: Weather and Climate
903 Extreme Events in a Changing Climate, in: *Climate Change 2021: The Physical Science Basis. Contribution of*
904 *Working Group I to the Sixth Assessment Report of the Intergovernmental Panel on Climate Change*, edited by:
905 Masson-Delmotte, V., Zhai, P., Pirani, A., Connors, S. L., Péan, C., Berger, S., Caud, N., Chen, Y., Goldfarb, L.,
906 Gomis, M. I., Huang, M., Leitzell, K., Lonnoy, E., Matthews, J. B. R., Maycock, T. K., T. Waterfield, Yelekçi, O.,
907 Yu, R., and Zhou, B., Cambridge University Press, Cambridge, 2021.
- 908 Simley, J. D. and Carswell Jr, W. J.: *The National Map-Hydrography Using the Data: Fact Sheet 2009-3054*, 2010.
- 909 Skougaard Kaspersen, P., Høegh Ravn, N., Arnbjerg-Nielsen, K., Madsen, H., and Drews, M.: Comparison of the
910 impacts of urban development and climate change on exposing European cities to pluvial flooding, *Hydrol Earth*
911 *Syst Sci*, 21, 4131–4147, <https://doi.org/10.5194/HESS-21-4131-2017>, 2017.
- 912 Smith, A., Bates, P. D., Wing, O., Sampson, C., Quinn, N., and Neal, J.: New estimates of flood exposure in
913 developing countries using high-resolution population data, *Nat Commun*, 10, 1814, [https://doi.org/10.1038/s41467-](https://doi.org/10.1038/s41467-019-09282-y)
914 [019-09282-y](https://doi.org/10.1038/s41467-019-09282-y), 2019.
- 915 Smith, J. A., Sturdevant-Rees, Paula., Baeck, M. Lynn., and Larsen, M. C.: Tropical cyclones and the flood
916 hydrology of Puerto Rico, *Water Resour Res*, 41, 1–16, <https://doi.org/10.1029/2004WR003530>, 2005.
- 917 Storlazzi, C. D., Gingerich, S. B., Van Dongeren, A., Cheriton, O. M., Swarzenski, P. W., Quataert, E., Voss, C. I.,
918 Field, D. W., Annamalai, H., Piniak, G. A., and Mccall, R.: Most atolls will be uninhabitable by the mid-21st
919 century because of sea-level rise exacerbating wave-driven flooding, *Sci Adv*, 4, 2018.
- 920 Swain, D. L., Wing, O. E. J., Bates, P. D., Done, J. M., Johnson, K., and Cameron, D. R.: Increased flood exposure
921 due to climate change and population growth in the United States, *Earths Future*, 8,
922 <https://doi.org/10.1029/2020ef001778>, 2020.
- 923 Tanaka, T., Kiyohara, K., and Tachikawa, Y.: Comparison of fluvial and pluvial flood risk curves in urban cities
924 derived from a large ensemble climate simulation dataset: A case study in Nagoya, Japan, *J Hydrol (Amst)*, 584,
925 <https://doi.org/10.1016/j.jhydrol.2020.124706>, 2020.
- 926 Tatem, A. J.: WorldPop, open data for spatial demography, <https://doi.org/10.1038/sdata.2017.4>, 31 January 2017.
- 927 Thomas, A., Pringle, P., Pflleiderer, P., and Schleussner, C.-F.: *Tropical Cyclones: Impacts, the link to Climate*
928 *Change and Adaptation*, New York, 2017.
- 929 Thomas, A., Shooya, O., Rokitzki, M., Bertrand, M., and Lissner, T.: Climate change adaptation planning in
930 practice: insights from the Caribbean, *Reg Environ Change*, 19, 2013–2025, [https://doi.org/10.1007/s10113-019-](https://doi.org/10.1007/s10113-019-01540-5)
931 [01540-5](https://doi.org/10.1007/s10113-019-01540-5), 2019.
- 932 Thomas, A., Baptiste, A. K., Baptiste, A., Martyr-Koller, R., Pringle, P., and Rhiney, K.: Climate Change and Small
933 Island Developing States, *Annu Rev Environ Resour*, 45, <https://doi.org/10.1146/annurev-environ-012320-083355>,
934 2020.



- 935 Tiecke, T. G., Liu, X., Zhang, A., Gros, A., Li, N., Yetman, G., Kilic, T., Murray, S., Blankespoor, B., Prydz, E. B.,
936 and Dang, H.-A. H.: Mapping the world population one building at a time, Washington D.C., 2017.
- 937 Towe, V., Petrun Sayers, E., Chan, E., Kim, A., Tom, A., Chan, W., Marquis, J., Robbins, M., Saum-Manning, L.,
938 Weden, M., and Payne, L.: Community Planning and Capacity Building in Puerto Rico After Hurricane Maria:
939 Predisaster Conditions, Hurricane Damage, and Courses of Action, RAND Corporation, Santa Monica,
940 <https://doi.org/10.7249/RR2598>, 2020.
- 941 Tuholske, C., Gaughan, A. E., Sorichetta, A., de Sherbinin, A., Bucherie, A., Hultquist, C., Stevens, F.,
942 Kruczkiewicz, A., Huyck, C., and Yetman, G.: Implications for Tracking SDG Indicator Metrics with Gridded
943 Population Data, *Sustainability*, 13, 7329, <https://doi.org/10.3390/su13137329>, 2021.
- 944 Uhe, P. F., Mitchell, D. M., Bates, P. D., Sampson, C. C., Smith, A. M., and Islam, A. S.: Enhanced flood risk with
945 1.5 °C global warming in the Ganges–Brahmaputra–Meghna basin, *Environmental Research Letters*, 14, 074031,
946 <https://doi.org/10.1088/1748-9326/ab10ee>, 2019.
- 947 United Nations Framework Convention on Climate Change: Adoption of the Paris Agreement, Paris, 2015.
- 948 United Nations Office for Disaster Risk Reduction: Global Assessment Report on Disaster Risk Reduction (5th ed.),
949 Geneva, 2019.
- 950 Terminology: <https://www.unisdr.org/we/inform/terminology>, last access: 28 October 2019.
- 951 United States Geological Survey: Commonwealth of Puerto Rico QL2 Lidar Report Produced for U.S. Geological
952 Survey, Tampa, 2017.
- 953 Vosper, E. L., Mitchell, D., and Emanuel, K.: Extreme Hurricane Rainfall affecting the Caribbean mitigated by the
954 Paris Agreement Goals, *Environmental Research Letters*, 15, <https://doi.org/10.1088/1748-9326/ab9794>, 2020.
- 955 Wehner, M. and Sampson, C.: Attributable human-induced changes in the magnitude of flooding in the Houston,
956 Texas region during Hurricane Harvey, *Clim Change*, 166, 20, <https://doi.org/10.1007/s10584-021-03114-z>, 2021.
- 957 Williams, G. P.: Bank-full discharge of rivers, *Water Resour Res*, 14, 1141–1154,
958 <https://doi.org/10.1029/WR014I006P01141>, 1978.
- 959 Willison, C. E., Singer, P. M., Creary, M. S., and Greer, S. L.: Quantifying inequities in US federal response to
960 hurricane disaster in Texas and Florida compared with Puerto Rico, *BMJ Glob Health*, 4,
961 <https://doi.org/10.1136/BMJGH-2018-001191>, 2019.
- 962 Wing, O. E. J., Bates, P. D., Sampson, C. C., Smith, A. M., Johnson, K. A., and Erickson, T. A.: Validation of a 30
963 m resolution flood hazard model of the conterminous United States, *Water Resour Res*, 53, 7968–7986,
964 <https://doi.org/10.1002/2017WR020917>, 2017.
- 965 Wing, O. E. J., Bates, P. D., Smith, A. M., Sampson, C. C., Johnson, K. A., Fargione, Joseph., and Morefield,
966 Philip.: Estimates of present and future flood risk in the conterminous United States, *Environmental Research*
967 *Letters*, 13, <https://doi.org/10.1088/1748-9326/aaac65>, 2018.
- 968 Wing, O. E. J., Sampson, C. C., Bates, P. D., Quinn, N., Smith, A. M., and Neal, J. C.: A flood inundation forecast
969 of Hurricane Harvey using a continental-scale 2D hydrodynamic model, *J Hydrol (Amst)*, 4,
970 <https://doi.org/10.1016/j.hydroa.2019.100039>, 2019.



- 971 Wing, O. E. J., Smith, A. M., Marston, M. L., Porter, J. R., Amodeo, M. F., Sampson, C. C., and Bates, P. D.:
972 Simulating historical flood events at the continental scale: observational validation of a large-scale hydrodynamic
973 model, *Natural Hazards and Earth System Sciences*, 21, 559–575, <https://doi.org/10.5194/nhess-21-559-2021>, 2021.
974 Wolman, M. G. and Miller, J. P.: Magnitude and Frequency of Forces in Geomorphic Processes, *J Geol*, 68, 54–74,
975 1960.
976 World Bank: Flood Hazards: Methodology Book, CHARIM: Caribbean Handbook on Disaster Risk Management,
977 2015.
978 World Meteorological Organization: State of the Global Climate 2021: WMO Provisional Report, Geneva, 2021.
979 Yamazaki, D., Ikeshima, D., Tawatari, R., Yamaguchi, T., O’Loughlin, F., Neal, J. C., Sampson, C. C., Kanae, S.,
980 and Bates, P. D.: A high-accuracy map of global terrain elevations, *Geophys Res Lett*, 44, 5844–5853,
981 <https://doi.org/10.1002/2017GL072874>, 2017.
982 Yamazaki, D., Ikeshima, D., Sosa, J., Bates, P. D., Allen, G. H., and Pavelsky, T. M.: MERIT Hydro: A High-
983 Resolution Global Hydrography Map Based on Latest Topography Dataset, *Water Resour Res*, 55, 5053–5073,
984 <https://doi.org/10.1029/2019WR024873>, 2019.
985 Zhou, G., Sun, Z., and Fu, S.: An efficient variant of the Priority-Flood algorithm for filling depressions in raster
986 digital elevation models, *Comput Geosci*, 90, 87–96, <https://doi.org/10.1016/j.cageo.2016.02.021>, 2016.
987 Zhu, L., Quiring, S. M., and Emanuel, K. A.: Estimating tropical cyclone precipitation risk in Texas, *Geophys Res*
988 *Lett*, 40, 6225–6230, <https://doi.org/10.1002/2013GL058284>, 2013.
989